Clay mineral–water interactions

4

Cliff T. Johnston
Departments of Earth, Atmospheric and Planetary Sciences and Agronomy, Purdue University, West Lafayette, IN, United States

4.1 Introduction

Water is comprised of two of the three most abundant elements in the Universe, and is the most abundant molecule found on the surface of the Earth to a depth of several thousand metres (Fraser et al., 2002; Mottl et al., 2007). The 'Blue Planet' is defined and controlled by the presence of water. It is the key compound for sustaining life on Earth. In some way, shape, or form, water is involved in the great majority of all geological, biological, and chemical processes. In geology, for example, the continual interaction of water with exposed mineral surfaces at the rock–water interface has produced a broad array of weathering products, including clay minerals (Hazen and Ferry, 2010). Thus, the interaction of water with 'high surface area to volume' clay minerals is critically important to many different disciplines, including all aspects of geology, soil, and water science, geotechnical engineering, geomorphology, seismology, geophysics, petroleum engineering, atmospheric science, and astrobiology.

In addition to being the most abundant molecule on the Earth's surface, it is also the most anomalous. The anomalous macroscopic properties of water are familiar and are clearly demonstrated in terms of its isobaric temperature dependence of density, thermal expansion coefficient, compressibility, and heat capacity (Debenedetti, 2003; Gallo et al., 2016). As shown in Fig. 4.1, the density of water reaches a maximum at 4°C, and the solid phase has lower density than that of the liquid (i.e. ice floats). Both the isothermal compressibility and heat capacity of 'simple liquids' increase with increasing temperature. In the case of water, however, these quantities increase with decreasing temperature. The isothermal compressibility and specific heat of water reach minima at 46°C and 35°C, respectively (Fig. 4.1). Although these unusual properties of water are well known, the underlying static and dynamic properties of water remain a current area of research (Pettersson et al., 2016). These properties are attributed to entropy and volume fluctuations in the structure of water that increase upon cooling, in the case of water. These have been described as a 'cascade of anomalies' which, in turn, lead to the unusual response of the thermodynamic properties (Gallo et al., 2016).

The interaction of water with ions is central to understanding clay mineral–water interactions. From a thermodynamic perspective, it is useful to consider the stepwise interaction of H_2O with selected alkali metal cations to illustrate the concept of the enthalpy of hydration. As shown in Table 4.1, the change in enthalpy for one H_2O molecule associating with Li^+ is -142 kJ/mol, the second H_2O molecule contributes another -100 kJ/mol. Negative enthalpy values mean that heat is released during the

Developments in Clay Science, Vol. 9. https://doi.org/10.1016/B978-0-08-102432-4.00004-4

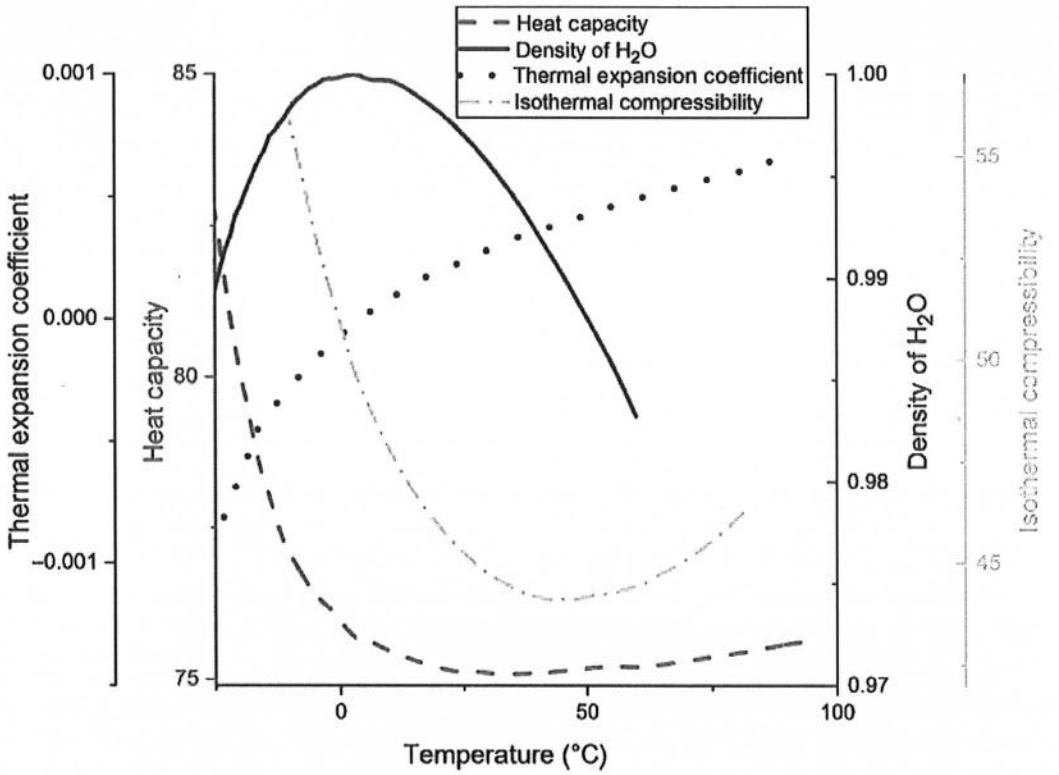

Fig. 4.1 Anomalous behaviour of water as a function of temperature: thermal expansion coefficient (α_p units of K^{-1} shown in *black*; *dotted line* in print version), specific heat capacity (C_p units J K^{-1} mol^{-1} shown in *red*; *dashed line* in print version), density (ρ units of g cm^{-3} shown in *blue*; *solid line* in print version), isothermal compressibility (K_T units of bar^{-1} shown in *green*; *dash-dot line* in print version).
Adapted from Angell, C.A., Oguni, M., Sichina, W.J., 1982. Heat capacity of water at extremes of supercooling and superheating. *Journal of Physical Chemistry*, 86, 998–1002; Debenedetti, P.G., 2003. Supercooled and glassy water. J. Phys. Condens. Matter, 15, R1669–R1726.

reaction. The cumulative change in enthalpy after complexation by six H_2O molecules is −515 kJ/mol, which is close to the 'infinite' hydration, or the Standard Molar Enthalpy of Hydration ($-\Delta_h H_I^\infty$), value of −531 kJ/mol (Marcus, 1987, 2015a). Stepwise hydration data are also presented for Na^+ and K^+ in Table 4.1. Standard molar enthalpies, entropies, and free energies for a broader suite of ions are listed in Table 4.2, and the following trends can be observed. For both the alkali and alkaline earth metal cations, the $-\Delta_h H_I^\infty$ values become less negative with increasing atomic numbers within a given row. The cations with the smaller ionic radii (e.g. Li^+ or Mg^{2+}) have larger negative enthalpies of hydration compared with their larger counterparts (e.g. Cs^+ and Ba^{2+}), meaning these smaller cations associate with water more strongly. Second, the $-\Delta_h H_I^\infty$ values become more negative with increasing valence. For example, the $-\Delta_h H_I^\infty$ values for Na^+, Mg^{2+}, and Al^{3+} for the Period 3 elements are −416, −1949, and −4715 kJ/mol, respectively.

Also included in Table 4.2 are the molar structural entropies for some of the ions. A molar structural entropy change is defined that measures the change in the structural

Table 4.1 The standard molar enthalpies of stepwise clustering of water molecules around ions in the ideal gas phase, $-\Delta_{n-1,n}H°$/kJ/mol, at $T° = 298.15\,K$

	Li^+		Na^+		K^+	
	Stepwise hydration enthalpy (kJ/mol)	Cumulative hydration enthalpy (kJ/mol)	Stepwise hydration enthalpy (kJ/mol)	Cumulative hydration enthalpy (kJ/mol)	Stepwise hydration enthalpy (kJ/mol)	Cumulative hydration enthalpy (kJ/mol)
$M^+_{(g)} + H_2O = M(H_2O)^+_{(g)}$	−142		−100		−75	
$M(H_2O)^+_{(g)} + H_2O \rightarrow M(H_2O)_2^+{}_{(g)}$	−108	−250	−83	−183	−67	−142
$M(H_2O)_2^+{}_{(g)} + H_2O \rightarrow M(H_2O)_3^+{}_{(g)}$	−87	−337	−66	−249	−55	−197
$M(H_2O)_3^+{}_{(g)} + H_2O \rightarrow M(H_2O)_4^+{}_{(g)}$	−69	−406	−58	−307	−49	−246
$M(H_2O)_4^+{}_{(g)} + H_2O \rightarrow M(H_2O)_5^+{}_{(g)}$	−58	−464	−51	−358	−45	−291
$M(H_2O)_5^+{}_{(g)} + H_2O \rightarrow M(H_2O)_6^+{}_{(g)}$	−51	−515	−45	−403	−42	−333
Standard molar enthalpy of hydration (kJ/mol) $\Delta_h H_I^\infty$	Li^+	−531	Na^+	−416	K^+	−334

Data from Dzidic, I., Kebarle, P., 1970. Hydration of the alkali ions in the gas phase. Enthalpies and entropies of reactions M+(H2O) n-1 + H2O = M+(H2O)n. J. Phys. Chem. 74, 1466–1474; Marcus, Y., 2015. Ions and their properties. In: Ions in Solution and Their Solvation. John Wiley & Sons, Inc.

Table 4.2 Standard molar enthalpies, entropies, Gibb energies of hydration structural entropy, and B NMR and B viscosity terms

Ion	$-\Delta_h H_I^\infty$	$-\Delta_h S_I^\infty$	$-\Delta_h G_I^\infty$	$\Delta_{str}S_I$	B_{NMR}	B_η
	kJ/mol			J/mol	$dm^3\,mol^{-1}$	
Li^+	531	141.8	489	−52	0.14	0.146
Na^+	416	111.2	383	−14	0.06	0.085
K^+	334	74.3	312	47	−0.01	−0.009
Rb^+	308	65.1	289	52	−0.04	−0.033
Cs^+	283	58.6	266	68	−0.05	−0.047
Mg^{2+}	1949	331.2	1837	−113	0.5	0.385
Ca^{2+}	1602	252.4	1527	−59	0.27	0.284
Sr^{2+}	1470	241.7	1398	−53	0.23	0.261
Ba^{2+}	1332	208.2	1270	−18	0.18	0.216
Cr^{2+}	1933	308.1	1841			
Mn^{2+}	1874	291.8	1787			
Fe^{2+}	1972	362.4	−1864			
Al^{3+}	4715	538.5	4554			
Fe^{3+}	4462	556.1	−4296			

Data from Marcus, Y., 2015. Ions and their properties. In: Ions in Solution and Their Solvation. John Wiley & Sons, Inc.

order of an infinitely dilute solution caused by the introduction of the ion into the solvent (water, in this case). This value is obtained from the standard molar entropy of solvation of the ion, after certain unrelated quantities are subtracted (Marcus, 2009, 2015b). It is related to the qualitative terms 'kosmotropes' and 'chaotropes' (Collins, 1997, 2004; Collins et al., 2007) used to describe 'structure making' and 'structure breaking' ions. Kosmotropes are small ions of high charge density with the ability to bind strongly to water molecules. In contrast, chaotropes are larger ions of low charge density that have lower affinities for water (Collins, 1997). Similarly, Burgess introduced the term 'standard partial molar entropy,' which is based on the assumption of zero for the hydrated proton (Burgess, 1999). Conceptually, these terms emphasise the competition between water–water interactions and the perturbation introduced by the presence of the ion. Note that the hydration structural entropies ($\Delta strS_I$) are much smaller, with values that range from −113 for Mg^{2+} to +68 J/mol for Cs^+ (J/mol not kJ/mol). When small cations with high charge densities (e.g. Mg^{2+}) are added into water, it results in a large number of electrostricted water molecules (water molecules that are strongly associated with the cation), causing a decrease in entropy (−113 J/mol for Mg^{2+}). These cations are called 'structure making' ions. On the other hand, addition in water of ions having a large size and low charge density results in an increase in entropy. For example, Cs^+ introduced in water results in a $\Delta strS_I$ change of +68 J/mol, causing an increase in entropy, and thus Cs^+ is classified as a 'structure breaking' ion. A list of structure making and structure breaking ions (Marcus, 2009) is presented in Table 4.3.

Two additional terms are listed in Table 4.2 that provide insight about how a particular ion influences the structure of water.

Table 4.3 A partial list of structure making and structure breaking ions (Marcus, 2009)

Structure breaking ions
I^-, ClO_4^-, MnO_4^-, TcO_4^-, $Cr_2O_7^{2-}$, Br^-, SCN^-, Cl^-
K^+, Rb^+, Cs^+, Tl^+, CN^-, NO_2^-, NO_3^-, $Al(OH)_4^-$, S^{2-}, $(CH_3)_4N^+$,
Ra^{2+}, HCO_2^-, HSO_4^-, SeO_4^{2-}, CrO_4^{2-}, NH_4^+, $B(OH)_4^-$, SO_4^{2-}, MoO_4^{2-}, WO_4^{2-}, $C_2O_4^{2-}$
Borderline ions
Na^+, Ag^+, Ba^{2+}, Pb^{2+}, F^-, HCO_3^-, $H_2PO_4^-$
Structure making ions
Li^+, Sr^{2+}, Sn^{2+}, Al^{3+}, Cr^{3+}, Bi^{3+}, OH^-, Ca^{2+}, Eu^{2+}, Hg_2^{2+}, Sc^{3+}, Co^{3+}, Pu^{4+}, HPO_4^{2-}
V^{2+}, Cr^{2+}, Mn^{2+}, Cu^{2+}, Cd^{2+}, Fe^{3+}, AsO_4^{3-}
Mg^{2+}, Co^{2+}, Ni^{2+}, Zn^{2+}, Y^{3+}, La^{3+} to Eu^{3+}, $PO4^{3-}$, Fe^{2+}, UO_2^{2+}

(i) The first is the viscosity B_η coefficient that is part of the Jones–Dole expression to calculate the relative viscosity changes of water in the presence of a particular ion:

$$\left[\left(\frac{\eta}{\eta^*}\right) - 1\right] = A_\eta c^{1/2} + B_\eta c + \ldots$$

Different types of ions can increase or decrease the viscosity of water, and this concept is captured in the B_η coefficient (dm^3/mol). Li^+, for example, causes the viscosity to increase, whereas Cs^+ results in a decrease in viscosity.

(ii) Analogous to the viscosity B_η coefficient, is the NMR longitudinal proton relaxation time B_{NMR} (dm^3 /mol). NMR relaxation times are longer from structure-making ions and shorter from structure-breaking ions. Proton (^1H) NMR longitudinal relaxation times are restricted to diamagnetic ions. The alkali metal cations, that is, Li^+, Na^+, K^+, Rb^+, and Cs^+ all are diamagnetic due to the absence of unpaired electrons. For paramagnetic transition metal cations, ^{17}O NMR spin–lattice relaxation of D_2O can be used to look at water reorientation.

When considering molecular properties of water and hydrated ions, it is important to consider the timescale associated with a particular experimental method (Sposito and Prost, 1982; Guven, 1992). Vibrational transitions, for example, occur in the timescale from 10^{-15} to 10^{-12} s and NMR transitions are considerably slower (10^{-11} to 10^{-3} s). Thus, a molecular motion may appear to be static using vibrational spectroscopy, whereas a motion-averaged structure may be observed in NMR, EPR, or neutron scattering.

The ratio of reorientation times of hydration water molecules in 1 M salt solutions to that of pure water (Table 4.4) is determined using dielectric relaxation (Giese et al., 1970; Marcus, 2009). The reorientation time increases with decreasing cation size. The structure of ionic hydration shells has been explored using a diverse suite of

Table 4.4 Ratio of H_2O reorientation times of ion in 1 M salt solution (τ_{IM}) to that in pure H_2O (τ_W)

Ion	τ_{IM}/τ_w	Ion	τ_{IM}/τ_w
Li^+	2.41	F^-	2.61
Na^+	1.53	Cl^-	0.90
K^+	0.90	Br^-	0.73
Rb^+	0.78	I^-	0.41
Cs^+	0.68	OH^-	2.44
H_3O^+	1.62	NO_3^-	0.73
NH_4^+	0.72		
Me_4N^+	1.59		
Et_4N^+	1.96		
Pr_4N^+	2.37		
Bu_4N^+	2.80		

Data from Marcus, Y., 2009. Effect of ions on the structure of water: structure making and breaking. Chem. Rev. 109, 1346–1370.

methods, including X-ray and neutron diffraction, elastic and inelastic neutron scattering, vibrational, EXAFS, NMR, and dielectric relaxation spectroscopies, and molecular simulation (Ohtaki and Radnai, 1993; Marcus, 2009, 2015a; Van der Vegt et al., 2016).

Because water is a polar molecule, it interacts favourably with ions and other polar solutes in solution through Coulombic interactions. Neutron diffraction studies revealed that water molecules coordinated to metal ions through orientation of the oxygen atom towards the cation. $NiCl_2$, for example, revealed a Ni—O distance of 0.207 nm. The diameter of a water molecule has a radius of 0.140 nm, the corresponding ionic radius of the Ni^{2+} ion is 0.067 nm (Soper et al., 1977; Marcus, 1988; Ohtaki and Radnai, 1993). For water molecules coordinating to anions, the opposite orientation was found, as illustrated in Fig. 4.2.

The structure and dynamics of the complex hydrogen-bond (HB) network formed by water molecules is an area of active study using both static and advanced time resolved vibrational spectroscopies (Perakis et al., 2016). Vibrational spectroscopy provides unique information about the HB network and its dynamics. Linear FTIR and Raman spectra of neat and isotopically dilute water (e.g. HOD in D_2O) reveal insight about HB strength and the complex coupling of vibrational modes. In addition, ultra-fast time-resolved vibrational methods (pump-probe, photon-echo,

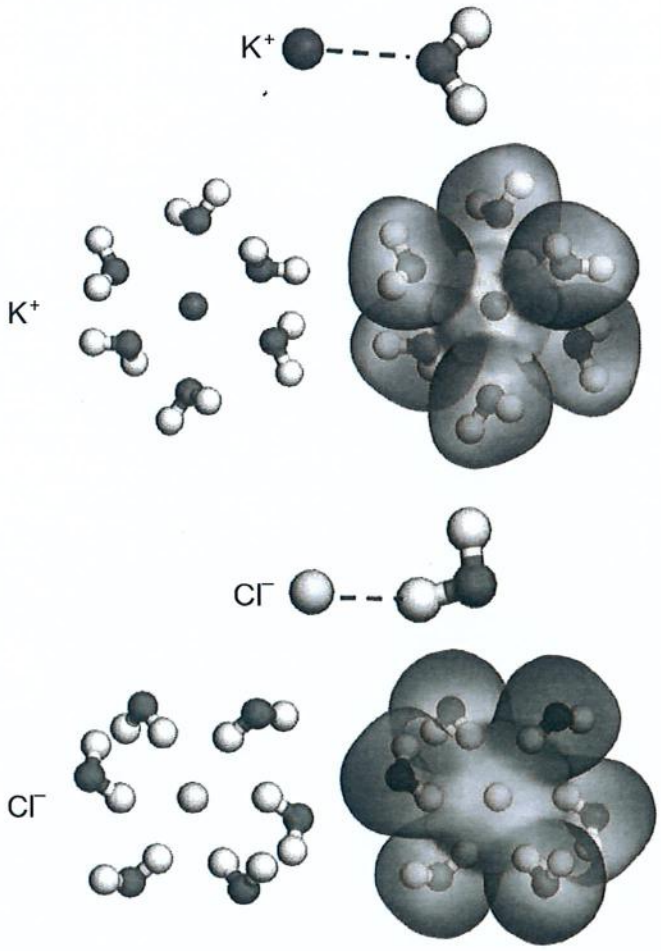

Fig. 4.2 Representation of H_2O molecules clustered around K^+ and Cl^- ion. Note orientation of the oxygen atoms of H_2O towards the K^+ ion and opposite orientation for H_2O molecules clustered around Cl^-. Images on the *right* correspond to an electrostatic potential map of the structures shown on the *left* where *blue* (*light grey* in the print version) shows partial negative charge and *red* (*dark grey* in the print version) represents partial positive charge.

and two-dimensional infrared (2D-IR)) can resolve transitions ranging from femtoseconds to nanoseconds and provide insights into the dynamics of the HB network and vibrational energy redistribution (Auer et al., 2007; Auer and Skinner, 2008; Li and Skinner, 2010b; Tainter et al., 2013; Ni and Skinner, 2015; Perakis et al., 2016; Götte et al., 2017). In addition, interface-specific techniques such as sum frequency generation (SFG) can probe the molecular structure of water and ions at both liquid–air and solid–liquid interfaces (Du et al., 1994; Hua et al., 2014; Ni and Skinner, 2015; DeWalt-Kerian et al., 2017; Götte et al., 2017). These experimental advances are helping to develop accurate molecular models of water and ions and solutes dissolved in water, and the behaviour of water at interfaces (Auer and Skinner, 2008; Li and Skinner, 2010a,b).

4.2 Water interactions with 'neutral clay mineral surfaces'

4.2.1 Talc and pyrophyllite

The interaction of water with clay minerals is complex and is influenced by the nature of the clay mineral surface, extent and location of isomorphous substitution, type of exchangeable cations, pH, ionic composition of the aqueous phase, particle size and shape, and the overall pore size distribution. The simplest systems to consider are talc and pyrophyllite, the 2:1 clay minerals that do not possess permanent structural charge, and have hydrophobic basal surfaces. Understanding how water interacts with these surfaces is important because these surface features are also present on with other clay minerals (e.g. kaolin group minerals) and on the neutral surfaces between isomorphous heterovalent substitution (IHS) sites of permanently charged clay minerals (e.g. smectites).

The structures of talc ($Si_4Mg_3O_{10}(OH)_2$) and pyrophyllite ($Si_4Al_2O_{10}(OH)_2$) are shown in Fig. 4.3 (refined structures based respectively on Lee and Guggenheim, 1981; Perdikatsis and Burzlaff, 1981). Talc is a trioctahedral mineral, meaning that

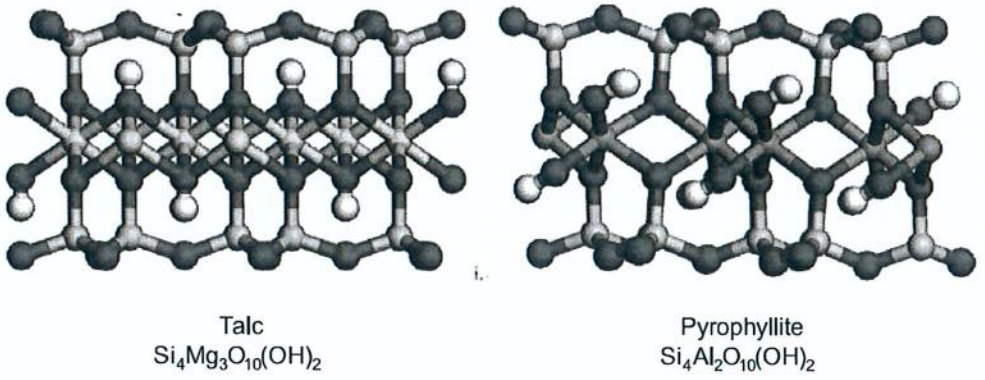

Fig. 4.3 Crystal structures of talc and pyrophyllite projected along [100]. The octahedral cation in talc is Mg^{2+} and that in pyrophyllite is Al^{3+}.
Structures refined from Lee, J.H., Guggenheim, S., 1981. Single-crystal X-ray refinement of pyrophyllite-1TC. Am. Mineral. 66, 350–357; Perdikatsis, B., Burzlaff, H., 1981. Structural refinement of talc $Mg_3(OH)_2Si_4O_{10}$. Z. Kristallogr. 156, 177–186.

all of the octahedral sites are occupied by a divalent cation (i.e. Mg^{2+}); the orientation of the OH is perpendicular to the clay mineral surface (Fig. 4.3). In contrast, only two out of the three possible octahedral sites in pyrophyllite are occupied by a trivalent ion, and the hydroxyl group is tilted towards the vacant site (Fig. 4.3).

Interaction of water with talc and pyrophyllite has been investigated using water adsorption isotherms (Michot et al., 1994; Malandrini et al., 1997; Douillard et al., 2002; Tarasevich, 2007), immersion calorimetry (Michot et al., 1994; Malandrini et al., 1997; Douillard et al., 2002), contact angle measurements (Schrader and Yariv, 1990; Giese et al., 1991; Malandrini et al., 1997; Douillard et al., 2002), atomic force microscopy (AFM) (Yan et al., 2013), Raman and IR spectroscopy (Rashchenko et al., 2016), and thermal analysis with evolved gas analysis (Michot et al., 1994). Water vapour adsorption isotherms on talc (and kaolinite) are shown in Fig. 4.4 (Douillard et al., 2002; Tarasevich, 2007), showing that water has an overall low affinity for talc, but does exhibit some hydrophilic character at low relative vapour pressure of H_2O. These results are supported by recent molecular modelling studies of H_2O-talc/pyrophyllite interactions (Wang et al., 2009; Rotenberg et al., 2011; Zeitler et al., 2012; Tarasevich and Aksenenko, 2014; Zarzycki and Gilbert, 2016). Both talc and pyrophyllite have low N_2 specific surface areas (2–18 m^2/g), low H_2O monolayer adsorption values (0.017–0.055 mmol H_2O/g), moderate H_2O cross-sectional areas (surface area occupied by one H_2O molecule nm^2/molecule), intermediate enthalpy of immersion values (mJ/m^2), and experimentally measured advancing contact angles ranging from 29 to 83 degrees (Schrader and Yariv, 1990; Giese et al., 1991; Michot et al., 1994; Malandrini et al., 1997; Douillard et al., 2002; Tarasevich, 2007).

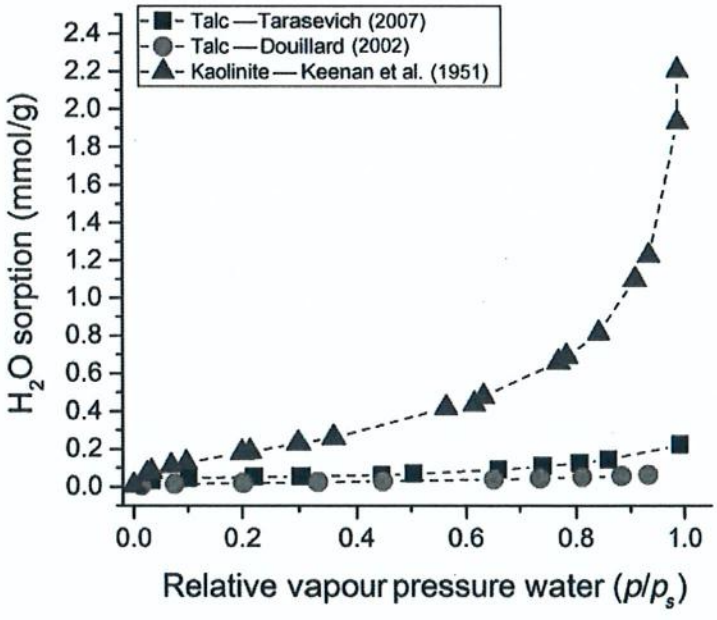

Fig. 4.4 Water vapour adsorption isotherms on talc and kaolinite.
Data read from plots in Keenan, A.G., Mooney, R.W., Wood, L.A., 1951. The relation between exchangeable ions and water adsorption on kaolinite. J. Phys. Colloid Chem. 55, 1462–1474; Douillard, J.M., Zajac, J., Malandrini, H., Clauss, F., 2002. Contact angle and film pressure: study of a talc surface. J. Colloid Interface Sci. 255, 341–351; Tarasevich, Y.I., 2007. The surface energy of hydrophilic and hydrophobic adsorbents. Colloid J. 69, 212–220.

There is general agreement that the basal surfaces of talc and pyrophyllite are hydrophobic, and the edges are hydrophilic. Due to their intrinsically small particle size, measurement of contact angles on a single crystal surface of talc and pyrophyllite is not possible. However, wicking and thin film measurements have yielded consistent results with values of 79–80 degrees (hydrophobic range) (Giese et al., 1991). Lower values have been reported in the literature for some samples, and this has been ascribed to the varying contribution of hydrophilic edge sites (Douillard et al., 1994; Tarasevich, 2007). For strongly dehydrated talc samples, both experimental and molecular modelling studies have shown an affinity of H_2O for the siloxane surface (Michot et al., 1994; Rotenberg et al., 2011). In the absence of water (e.g. strongly desiccated surface), talc behaves as a hydrophilic mineral (Michot et al., 1994). Quantitative thermal desorption measurements show that water is strongly retained by the surface, and immersion calorimetry measurements show a greater enthalpy of immersion for strongly dehydrated surfaces (Michot et al., 1994). These results are further supported by recent molecular modelling results, showing that H_2O has a high affinity of the basal surface at low surface coverage (Wang et al., 2009; Rotenberg et al., 2011). At low surface coverage, adhesive (water-surface) interactions out-compete cohesive (water–water interactions) and surface functions as a hydrophilic surface (Fig. 4.4). Classical density functional theory calculations have shown that H_2O adsorbed on pyrophyllite is oriented with the water dipole extending from the oxygen atom to the centre of mass of the hydrogen atoms, pointing away from the surface (Jeanmairet et al., 2014). At higher surface coverage of H_2O, cohesion (water–water) forces between water molecules out-compete the surface-water interactions, resulting in a strongly hydrophobic surface at higher water coverage, and calculated contact angles of 96 and 105 degrees for talc and pyrophyllite, respectively (Rotenberg et al., 2011). These results are consistent with the observed water vapour adsorption isotherms on talc (Fig. 4.4) that show an overall low affinity of talc for H_2O but with high affinity at low surface coverage (Michot et al., 1994; Douillard et al., 2002; Tarasevich, 2007). In addition, the cross-sectional surface areas derived from these water adsorption isotherms reveal values between 0.15 and 0.18 nm^2/H_2O molecules at monolayer coverage. For strongly hydrophobic surfaces, much larger values are generally observed.

Additional insight about the nature of the basal and edge surfaces of talc comes from force measurements on talc (and muscovite) particles using AFM combined with DLVO theory (Yan et al., 2013). DLVO is a dispersion stabilisation theory named after Derjaguin, Landau, Verwey, and Overbeek (see Derjaguin and Landau, 1941; Verwey and Overbeek, 1948). AFM-derived Stern potential measurements of the basal surface of both talc and muscovite were negative for all three ionic strengths, with the surface of muscovite showing a more negative charge (Fig. 4.5). The edge sites were less negative in distilled H_2O, and charge reversal was observed for Ca^{2+} and Mg^{2+} at higher ionic strength (Fig. 4.5).

Although talc is considered as a hydrophobic mineral under ambient conditions, talc–water interactions become important at elevated temperature and pressure. Under these conditions, talc reacts with H_2O to form a 10 Å phase (abbr. 'TAP'

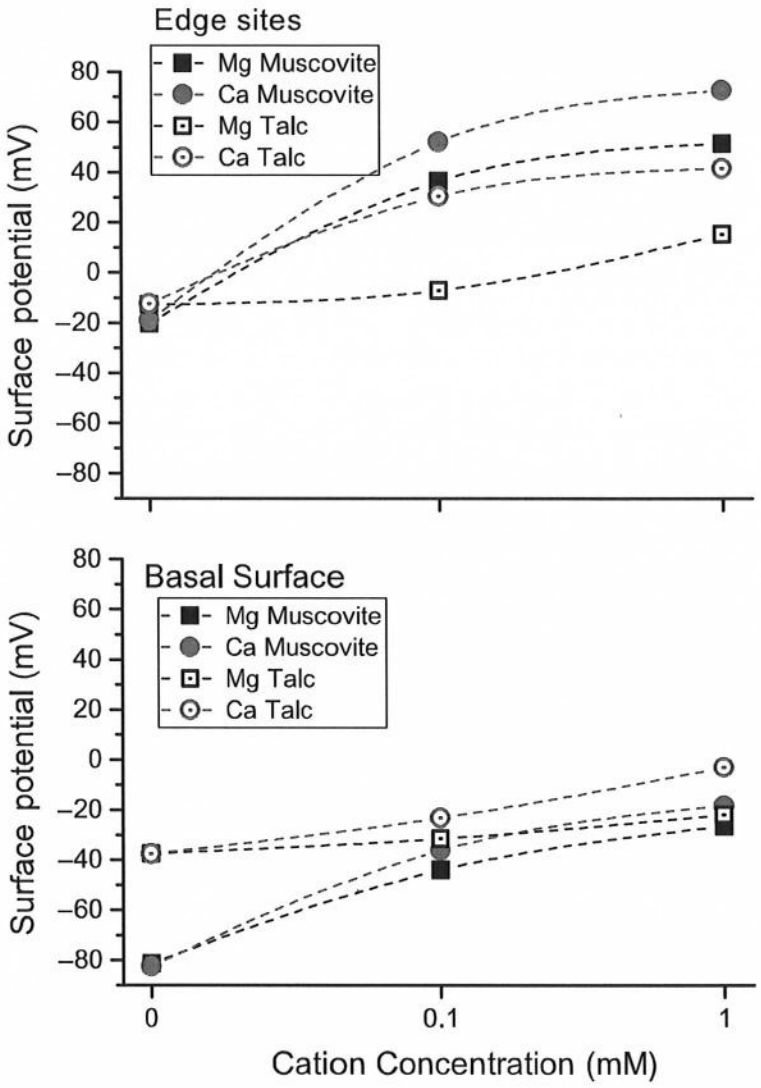

Fig. 4.5 AFM and DLVO-derived surface potentials of muscovite and talc basal planes and edges surfaces. Data read from plot in Yan, L.J., Masliyah, J.H., Xu, Z.H., 2013. Interaction of divalent cations with basal planes and edge surfaces of phyllosilicate minerals: muscovite and talc. J. Colloid Interface Sci. 404, 183–191.

for Ten Ångstrom Phase) with implications to serve as a host of water in subduction zones (Chinnery et al., 1999; Parry et al., 2007; Pawley and Welch, 2014; Rashchenko et al., 2016). A combination of high pressure Raman, XRD, and IR methods have revealed the transformation of talc to TAP. For example, the Raman spectrum of talc in the ν(OH) region is characterised by a sharp, well-resolved O—H stretching band at 3681 cm^{-1} corresponding to the ν(OH) mode of the structural OH groups. In the presence of H_2O at elevated temperature (500°C) and pressure (8 GPa), the 3681 cm^{-1} band is replaced by the two TAP ν(OH) bands at 3590 and 3631 cm^{-1} (Rashchenko et al., 2016). Similar spectral perturbations are observed using IR spectroscopy and XRD (Parry et al., 2007; Pawley and Welch, 2014).

4.2.2 Kaolin group mineral

Similar to talc and pyrophyllite, the 1:1 clay minerals do not possess significant structural charge, that is, little, if any, isomorphous substitution (Brigatti et al., 2013). This section will focus on the dioctahedral 1:1 structures of the kaolin group. The structure

of kaolin group minerals is based on the different arrangements of the structural unit of $Si_2Al_2O_5(OH)_4$ in the form of three main polytypes: kaolinite (most common), dickite, and nacrite (least common). In addition, halloysite is a hydrated form of kaolinite where one H_2O layer resides between the layers.

4.2.2.1.1 Kaolinite

The crystal structure of kaolinite (Kaol) is shown in Fig. 4.6. Unlike talc and pyrophyllite, Kaol is terminated by two different types of surfaces that produce an overall electrostatic dipole (Hu and Michaelides, 2010). As shown in Fig. 4.6, the top surface is a silica tetrahedral surface, similar to that found on pyrophyllite. The bottom surface is terminated by a 'gibbsite layer' of exposed Al–OH groups, similar to that of gibbsite.

The surfaces of the clay minerals and their interaction with H_2O have been investigated using an ever-increasing array of methods. Like most clay minerals, measuring the contact angle of water on Kaol is influenced by surface roughness, particle size, surface preparation, and pretreatment, temperature, and humidity (Yin and Miller, 2012). These values are generally not reliable. In this case, further complexity is introduced because Kaol has three types of surfaces. In addition to edge sites, the basal surface on the siloxane side of Kaol is hydrophobic, and the gibbsite-like surface is hydrophilic. Contact angle measurements vary from 15 to 46 degrees, reflecting the hydrophilic character of the gibbsite surface (Shang et al., 2010; Yin and Miller, 2012; Yin et al., 2012). This is also reflected by a wide variation in immersion

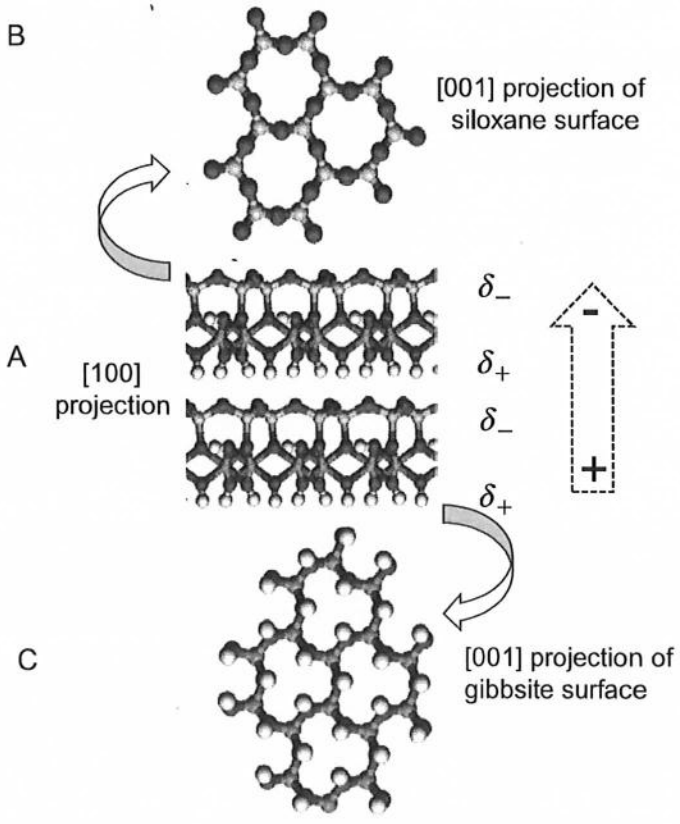

Fig. 4.6 Crystal structure of kaolinite (2 layers) projected along [100] (A). [001] projections showing the siloxane surface (B), and $[00\bar{1}]$ projection showing the gibbsite surface. Also shown are the partial positive charges on the gibbsite surface and partial negative charges of the siloxane surface resulting in an overall electrostatic dipole moment. Crystal structure from Bish, D.L., 1993. Rietveld refinement of the kaolinite structure at 1.5 K. Clays Clay Miner. 41, 738–744.

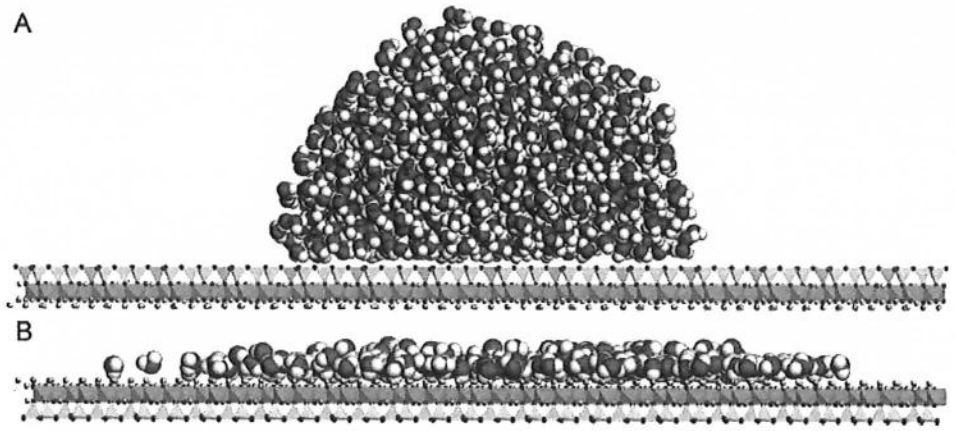

Fig. 4.7 Molecular dynamics simulation of a nanodrop of water in contact with the siloxane surface (A), and with the gibbsite surface (B) of kaolinite.
Illustration adapted from Solc, R., Gerzabek, M.H., Lischka, H., Tunega, D., 2011. Wettability of kaolinite (001) surfaces—molecular dynamic study. Geoderma 169, 47–54.

enthalpies ranging from -196 to $-308\,mJ/m^2$ (Partyka and Douillard, 1995; Douillard and Medout-Marere, 2000). Molecular dynamics simulations of nanodrops of water on the two surfaces of Kaol (Fig. 4.7) showed that the gibbsite surface was 'water wet' with a contact angle of $\sim 0°$ in contrast to the siloxane surface with a calculated contact angle of 105 degrees (Solc et al., 2011). Ions can also be introduced into nanopores to observe surface interactions (Vasconcelos et al., 2007). A simulated solution of CsCl was introduced to a nanopore within Kaol, and after 600 ps the ions had clearly segregated with the Cs^+ ions migrating to the siloxane surface, and the Cl^- ions to the opposing hydroxyl surface (Vasconcelos et al., 2007). High resolution AFM has provided further insight about the surface charge and charge distribution across particles of Kaol deposited on both sapphire and mica surfaces, exposing both silica and gibbsite surfaces, respectively (Kumar et al., 2016). It follows that the affinity of H_2O for Kaol is modest, but higher than that for talc (Fig. 4.4) (Keenan et al., 1951).

This dipolar nature of Kaol has led to recent interest in their role as Janus particles that can stabilise emulsions (Hirsemann et al., 2012; Weiss et al., 2013; Kirillova et al., 2014, 2016). Kaol has been successfully used to create Janus particles. These particles take advantage of the surface polarity differential between the siloxane and gibbsite surfaces. This allows each surface to be functionalised with different chemistries that can interact favourably with a hydrophobic phase on one side (e.g. oil) and an aqueous phase on the other.

4.2.2.1.2 Halloysite

The previous discussion focused on clay minerals that have minimal affinities for H_2O and whose overall water contents are generally less than 50 mg of H_2O/g of clay mineral. In the kaolin group minerals, halloysite (Hal) is a hydrated form of Kaol with 2 H_2O molecules per half unit cell intercalated between the siloxane surface of one layer and the gibbsite surface of the opposing layer (Fig. 4.8) with a structural formula

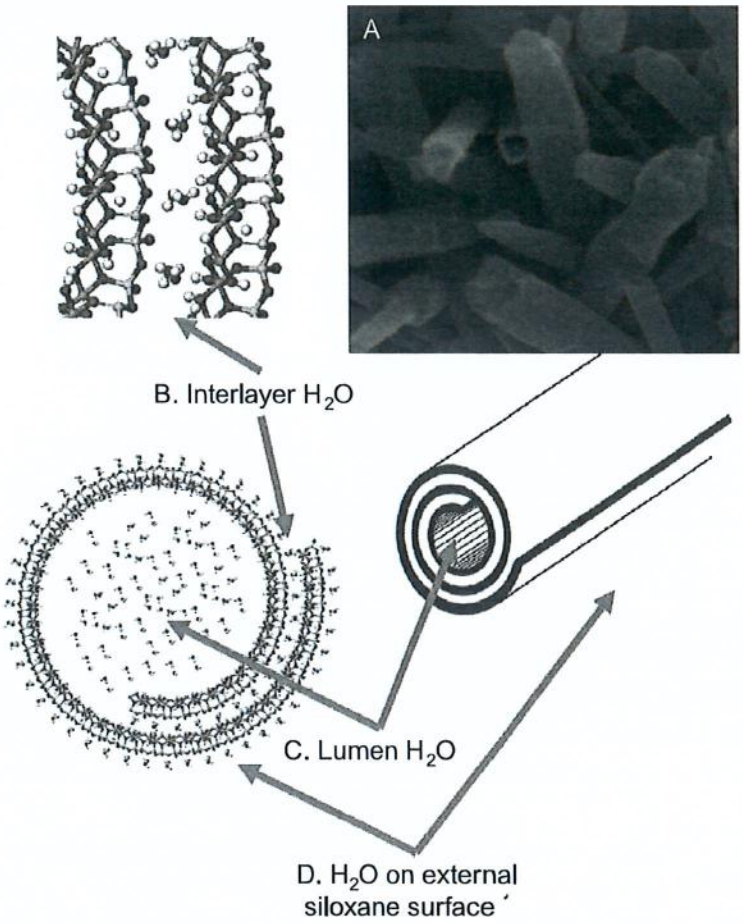

Fig. 4.8 Cryo-SEM micrograph and crystal structure of tubular halloysite showing three types of water. The cryo-SEM image (A) was obtained from a hydrated halloysite from the Gardner Mine Ridge deposit in Southern Indiana, USA (Ambers and Murray, 1995). Based on TEM analysis, the average inner diameter was ~15 nm and the outer diameter was 45–20 nm. A schematic of the tubular structure is shown in the *upper right portion*. The crystal structure of halloysite is from Ferrante et al. (2015). Three types of H_2O molecules are present, consisting of interlayer H_2O (B), H_2O present in the tubular structure or lumen (C), and H_2O external to the halloysite structure (D) (H_2O molecules not shown).
Data were adapted from Santagata, M.C., Premachandra, G.S., Johnston, C.T., 2009. Nanoconfined water in clay minerals. In: Mico et Nano Scientiae Mare Magnum. Castellaneta Marina (TA), Italy, AIPEA.

of $Si_2Al_2O_5(OH)_4(H_2O)_2$. Tubular morphology of Hal is the most common form (shown in Fig. 4.8); however, pseudo-spherical and spheroidal, platy or tubular, fibre, prismatic, and lath morphologies have been observed (Joussein et al., 2005). In addition to the H_2O molecules between the layers, water molecules are also found within the lumen (Fig. 4.8). Thermogravimetric analysis of Hal that is both fully hydrated and has never been dried has a mass loss of about 11.1 mmol H_2O/g of clay mineral. Loss of the two interlayer H_2O molecules (per $Si_2Al_2O_5(OH)_4$ unit) accounts for about 7.8 mmol H_2O/g of clay mineral. In addition, a loss of an additional 2.9 mmol H_2O/g of clay mineral was assigned to 'pore/lumen' water (Cruz et al., 1978).

Dehydration of Hal is irreversible due to the loss of the interlayer H_2O molecules (Bordallo et al., 2008). Although water will rehydrate the lumen, loss of interlayer H_2O is irreversible (Joussein et al., 2005).

Although Hal has been characterised extensively using IR and Raman spectroscopy (Janik and Keeling, 1993; Frost, 1995; Frost and Kristof, 1997; Frost and Shurvell, 1997; Kristof et al., 1997; Fialips et al., 2000; Adamo et al., 2001; Cuadros and Dudek, 2006; Zsirka et al., 2017), most of these studies examined dry samples that did not contain interlayer or lumen H_2O. A few studies have examined Hal samples containing both interlayer and lumen water (Tarasevi and Gribina, 1972; Yariv and Shoval, 1975; Johnston, 2017), which revealed that the interlayer and lumen water were somewhat more hydrogen bonded than in bulk water. Loss of interlayer water occurs rapidly, and a key point is that water should be considered as an integral part of the Hal structure (Johnston, 2017). In addition, the nanoconfined geometry of water in Hal is distinct from other strongly hydrated clay minerals in that interlayer cations are absent. The interlayer water molecules in Hal are interacting only with the siloxane and gibbsite surfaces, and with each other (Bordallo et al., 2008).

Neutron studies of Hal have revealed insight about the mobility of H_2O on the timescale of neutron scattering measurements. Common to many NMR and neutron studies of water mobility near clay mineral surfaces, the residence time between jumps, τ_0, of water in fully hydrated Hal was longer (7.1 ps) compared with that of bulk water (1.57 ps), and the corresponding self-diffusion coefficient was lower ($0.2–0.8 \times s10^{-9}$ m^2/s) compared with that of bulk water (2.49×10^{-9} m^2/s) (Bordallo et al., 2008). However, earlier studies showed that the specific heat of water in Hal was close to that of ice at temperatures <150 K, and was similar to that of liquid water at temperatures >250 K. Corresponding NMR measurements revealed that interlayer H_2O molecules rapidly rotated about their C_2 axis with a slower tumbling motion perpendicular to the C_2 axis (Cruz et al., 1978). Because different types of water molecules are present, the NMR and neutron data reflect contributions from both interlayer and lumen water. At present, there is significant interest in using Hal in a wide range of applications, taking advantage of its tubular structure and mesoporosity for applications in catalysis, drug delivery, and clay mineral polymer nanocomposites (Shchukin et al., 2005; Veerabadran et al., 2007; Lvov et al., 2008; Polansky et al., 2017; Zsirka et al., 2017).

4.3 Water interactions with 'charged clay mineral surfaces' (ion–dipole)

4.3.1 Smectites

Smectites are ubiquitous clay minerals that occur in soils, sediments, and rocks and control many important subsurface processes (Bergaya and Lagaly, 2013a,b). These clay minerals are strongly hydrated, and water is part of their structures. For example, attempts to remove all of the water from a smectite will generally result in the irreversible collapse of the clay mineral structure, and alteration of its surface properties.

The structure and properties of smectites have been reviewed extensively (Bergaya and Lagaly, 2013a; Brigatti et al., 2013; Emmerich, 2013; Schoonheydt and Johnston, 2013), and this section will focus on the interaction of water with smectites.

Smectites represent a diverse group of dioctahedral and trioctahedral planar 2:1 clay minerals with intermediate layer charge (χ) values ranging from 0.2 to 0.6 charges per formula unit. Isomorphous heterovalent substitution (IHS) that occurs in the crystal lattice produces a charge deficit within the crystal structure. Examples of IHS in smectites are shown in Fig. 4.9, illustrating Al^{3+} for Si^{4+} substitution in the tetrahedral sheet (common in saponite and beidellite) and Mg^{2+} for Al^{3+} substitution in the octahedral sheet (common in montmorillonite). The extent of IHS, also referred to as

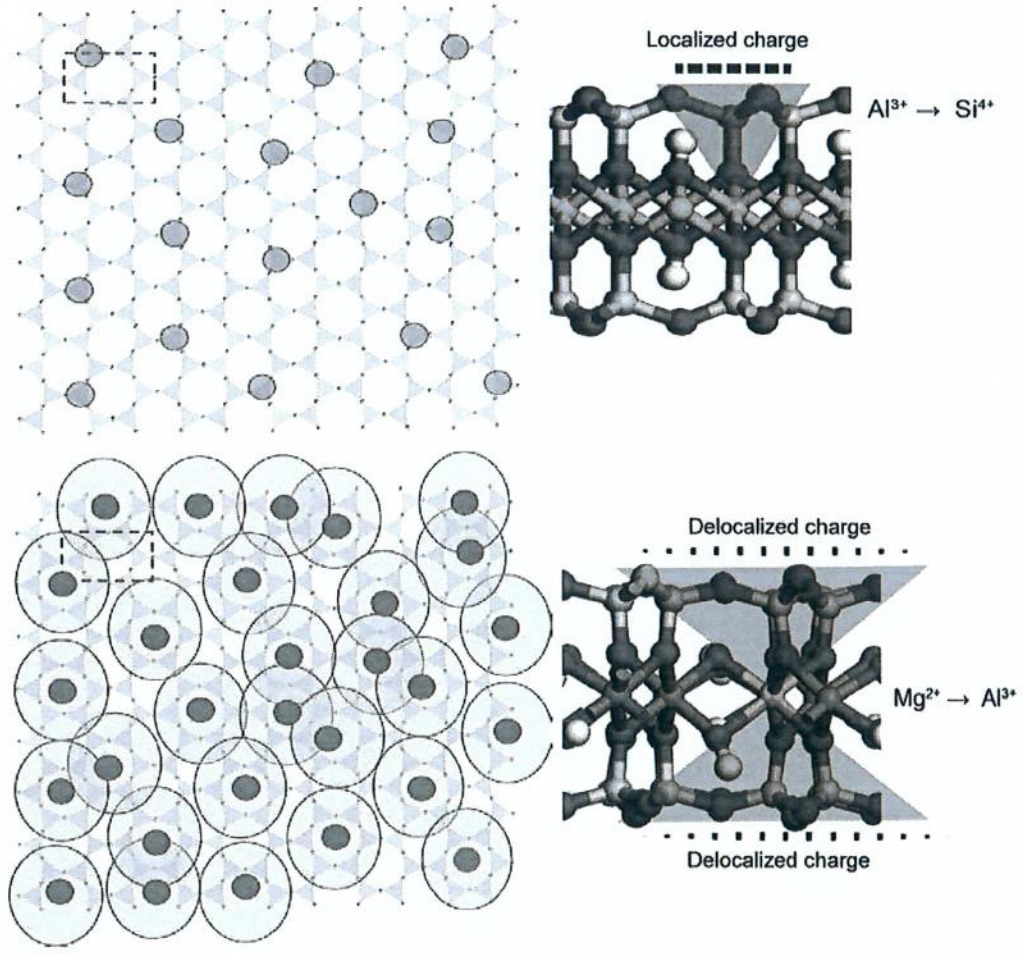

Fig. 4.9 Illustration of isomorphous heterovalent substitution (IHS) in the tetrahedral sheet ($Al^{3+} \rightarrow Si^{4+}$, *top right illustration*) and octahedral sheet ($Mg^{2+} \rightarrow Al^{3+}$, *lower right illustration*). The negative charge from IHS in the tetrahedral sheet is localised and is mainly manifest on one surface (*top surface* in this illustration). Looking down onto a 5 nm × 5 nm section of the basal surface, the distribution of the localised charges are conceptually illustrated by the *orange circles* (*grey* in the print version). In contrast, the charge from IHS in the octahedral sheet is delocalised over a larger number of oxygen atoms on both the *top* and *bottom surfaces* of layer. Because the charge is manifest on both surfaces, essentially the entire basal surface has some charged character.

structural charge, in a particular clay mineral is represented by χ, which corresponds to the number of IHSs in a half unit cell formula. Smectites are defined by the extent and type of IHS (Brigatti et al., 2013; Emmerich, 2013). In comparison with other types of clay minerals (kaolin group minerals, talc and pyrophyllite all have χ values of $\sim$0), vermiculites have higher layer charge ($0.6 < \chi < 0.9$), mica $\chi = 1$, and brittle micas have $\chi = 2$.

If the charge deficit created by IHS were point charges, the distance between the charge sites would vary between 0.6 and 1.2 nm for an isolated particle, depending on the surface charge density and type of IHS (Schoonheydt and Johnston, 2013; Johnston, 2017). However, because these substitutions occur within the crystal structure, the resultant negative charge will be distributed over a number of surface oxygen atoms on the siloxane surface. For tetrahedral substitution, the charge will be highly localised over a few oxygen atoms on 'one side' of the structure (Fig. 4.9). For IHS in the octahedral sheet, the charge will be distributed over a larger number of surface oxygen atoms on 'both sides' of the clay mineral structure (Fig. 4.9). Because the charge is more localised in smectites with tetrahedral substitution and the substitution is only manifest on one surface (as opposed to substitution in the octahedral sheet), a significantly greater proportion of the smectite surface will be 'neutral' and have similar properties to those of the pyrophyllite and talc surfaces reviewed earlier. This is illustrated in Fig. 4.9, comparing charge distribution in saponite and hectorite based on crude approximations of how the charge will be distributed over the surface oxygen atoms. Quantum chemical studies are beginning to provide additional information about how partial atomics charges are distributed on the surface oxygen atoms (Mignon et al., 2010; Lavikainen et al., 2015).

The negative structural charge deficit resulting from IHS is balanced by the presence of positively charged exchangeable cations in close proximity to the clay mineral surface illustrated in Fig. 4.10. The most common cations found in natural clay minerals are Ca^{2+}, Na^{+}, Mg^{2+} and K^{+}; however, the charge can be balanced by any positively charged ion, including H_3O^{+}, Al^{3+}, $Fe^{3+,2+}$, Cs^{+}, Sr^{2+}, or positively charged organic species. A distinguishing feature of the 'common' cations is that all have large negative enthalpies of hydration (Table 4.2), meaning that H_2O molecules are attracted to these interlayer cations, as shown in Fig. 4.10, resulting in the intrinsically high affinity of H_2O for smectites.

Water adsorption on smectites is generally high, although strongly dependent on the nature of the exchangeable cation, type, and extent of IHS. Key features of smectite–water are illustrated in Figs 4.11–4.13, comparing water adsorption isotherms for Na^{+}- and Ca^{2+}-montmorillonite (Mt) at different water contents (Prost et al., 1998). The lower figure plots the amount of water adsorbed in mmol H_2O/g vs the activity of water (a_w) (vapour pressure of H_2O/saturated vapour pressure of H_2O) ranging from 0 to 0.8 (p/p_s). The enthalpy of hydration of Ca^{2+} of -1669 kJ/mol is significantly higher than that of Na^{+} (-444 kJ/mol), resulting in more H_2O adsorbed to the Ca^{2+}-exchanged clay mineral in the crystalline swelling region (Fig. 4.11). The d-value of the Ca^{2+}-Mt at two different water contents is indicated. At an a_w value of 0.1, the d-value is 1.25 nm, corresponding to a one-layer hydrate, and at a_w value of 0.5, the d-value is 1.52 nm, corresponding to a two-layer hydrate. At a_w values > 0.98 p/p_s (osmotic

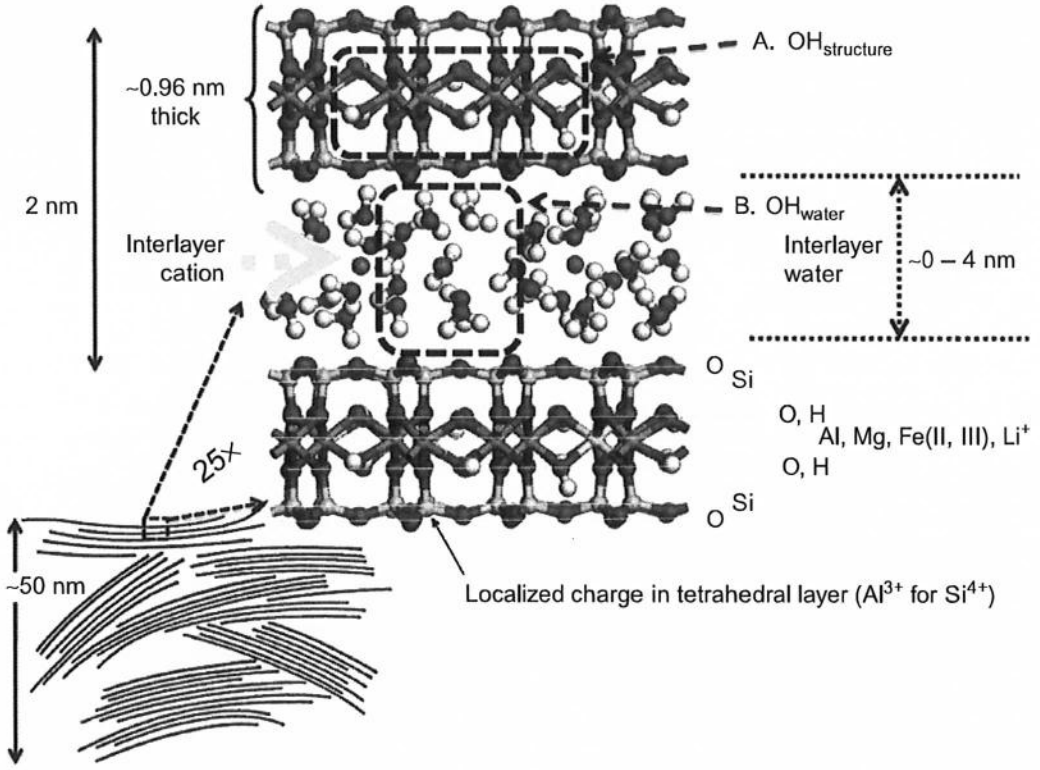

Fig. 4.10 Two montmorillonite particles with octahedral ISH separated by approximately three layers of H_2O. Interlayer H_2O molecules are clustered around exchangeable cations that balance the negative charge created by IHS. Also shown in the *lower left* is a conceptual view the morphology of montmorillonite particles stacked on top of each in the form of aggregates. Used with permission from Johnston, C.T., 2010. Probing the nanoscale architecture of clay minerals. Clay Miner. 45, 245–279.

swelling region), the situation is reversed, where the Na^+-exchanged clay mineral particles can be separated by larger distances, and more H_2O is associated with the Na^+-Mt at high a_w values (Prost et al., 1998). This is shown in Fig. 4.12 using $\log(\log(1/a_w))$ transformed x-axis to show the behaviour at high a_w values (see top axis in Fig. 4.12). In the high a_w range (>0.98), capillary condensation of H_2O occurs and the Na^+-exchanged clay mineral layers can swell to have d-values >5 nm (Norrish, 1954; Gilbert et al., 2015; Tester et al., 2016). Gilbert and coworkers have recently captured osmotic hydrates of Na^+-SWy-2 Mt using cryo-TEM and SAXS showing well-defined separations of particles as high as 60 nm (Gilbert et al., 2015; Tester et al., 2016).

The influence of the exchangeable cation on controlling water adsorption on smectites is shown in Fig. 4.13. Water desorption and adsorption isotherms for Na^+-, Ca^{2+}-, and Mg^{2+}-exchanged SAz-1 Mt in the region of crystalline swelling are shown in Fig. 4.13 (Johnston et al., 1992; Xu et al., 2000). SAz-1 Cheto Mt is a high surface charge density Mt with a χ value 0.47 and substitution almost exclusively in the octahedral sheet (Costanzo and Guggenheim, 2001; Srodon and McCarty, 2008). These isotherms reveal three important features of water adsorption to smectites: (i) the amount of water adsorbed is strongly influenced by the enthalpy of hydration of

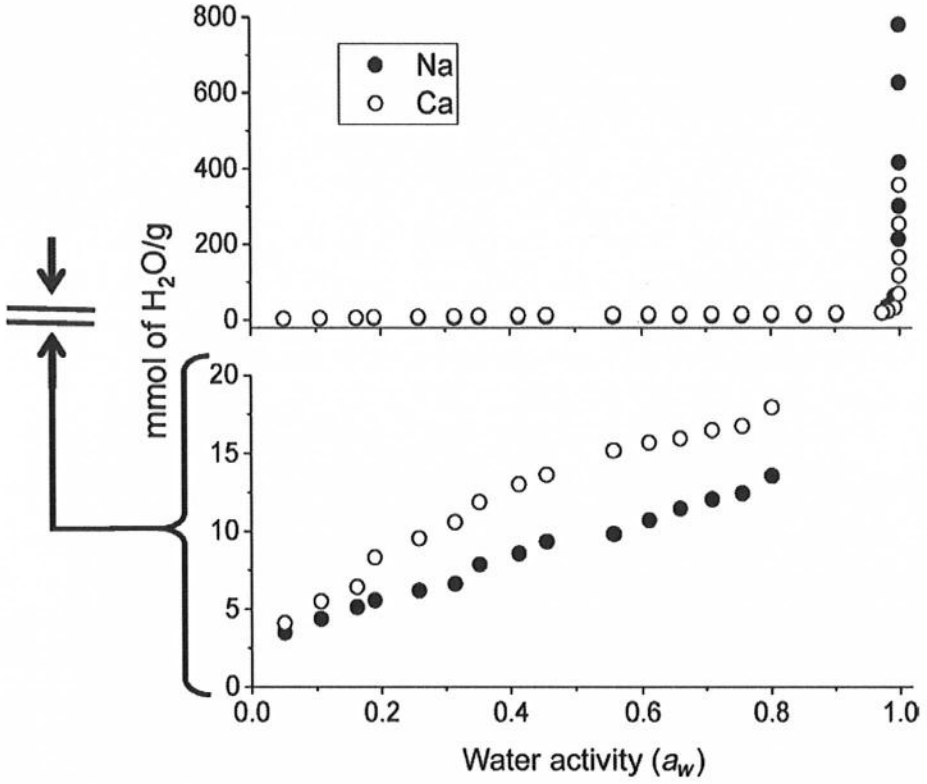

Fig. 4.11 Water adsorption isotherms of Na^+ and Ca^{2+} on montmorillonite. *Top figure* shows full range of relative vapour pressure of H_2O and water content, *lower plot* shows expanded range of 'crystalline swelling' in the $0 < a_w < 0.8$.
Data were read from plot in Prost, R., Koutit, T., Benchara, A., Huard, E., 1998. State and location of water adsorbed on clay minerals: consequences of the hydration and swelling-shrinkage phenomena. Clays Clay Miner. 46, 117–131.

the exchangeable cations with $Mg^{2+} > Ca^{2+} > Na^+$ (Table 4.2) in the domain of crystalline swelling (i.e. $0 < a_w < 0.9$); (ii) the desorption leg of the isotherm shows greater adsorption values related to the fact that it takes more energy to remove H_2O from the surface of the clay mineral than it does to adsorb it; (iii) the extent of hysteresis between the adsorption and desorption legs is related to the nature of the exchangeable cations. In the case of strongly hydrated cations, such as Mg^{2+}, the cations remain fully hydrated, and water has greater access to the interlayer spaces. In the case of less hydrated monovalent cations such as Na^+, the clay mineral layers can collapse to 1 W, or even 0 W hydrates. These clay minerals exhibit significant hysteresis because energy is required to rehydrate and separate the clay mineral layers. In a classic paper on smectite–water hysteresis, Mooney et al. (1952a,b) showed that water adsorption isotherms were not reliable because of this collapse-induced hysteresis, and that only desorption isotherms were reproducible. There have been numerous experimental studies of water adsorption to various smectites; examples include (Mooney et al., 1952a,b; Norrish, 1954; Hall and Astill, 1989; Cases et al., 1992, 1997; Johnston et al., 1992; Berend et al., 1996; Cancela et al., 1997; Xu et al., 2000; Schuttlefield et al., 2007a; Schnetzer et al., 2017). Water adsorption isotherms continue to play an important role in validating and benchmarking molecular simulation models.

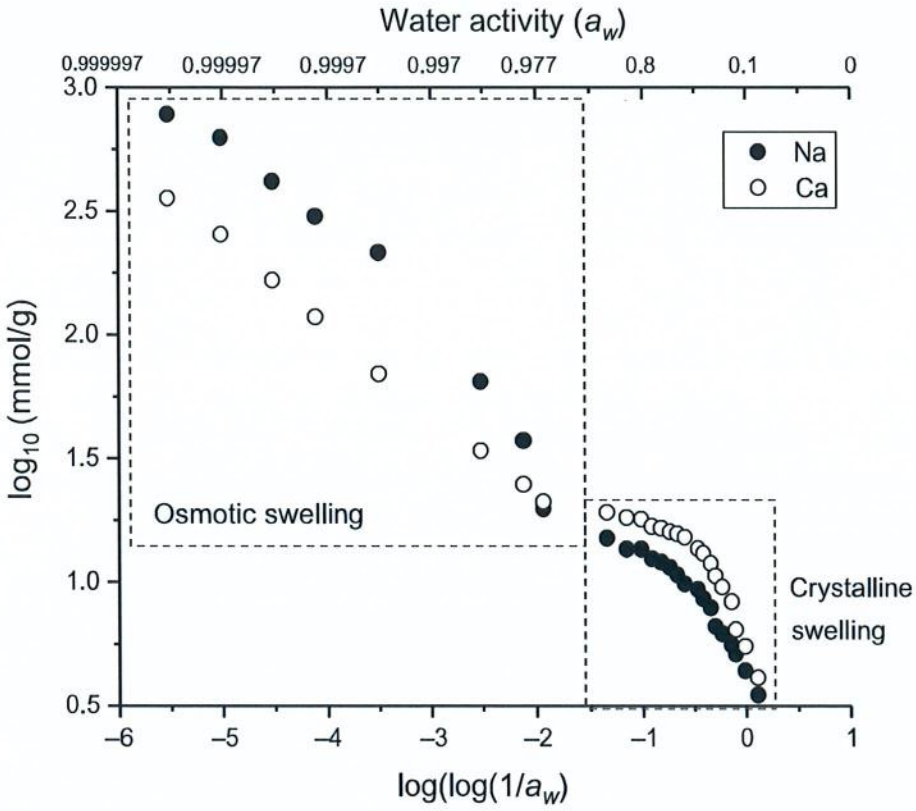

Fig. 4.12 Water adsorption isotherms of Na^+ and Ca^{2+} on montmorillonite using a $\log(\log(1/a_w))$ transformed x-axis. Actual relative vapour pressures of H_2O are shown on the top x-axis. Data were read from plot in Prost, R., Koutit, T., Benchara, A., Huard, E., 1998. State and location of water adsorbed on clay minerals: consequences of the hydration and swelling-shrinkage phenomena. Clays Clay Miner. 46, 117–131.

4.4 Molecular probe and reporter group studies of smectite–water interactions

Since the first reported IR study of water adsorbed to clay minerals more than 100 years ago (Coblentz, 1910, 1911), spectroscopic and related advanced characterisation methods have provided insight about how water interacts with clay mineral surfaces (Sposito and Prost, 1982; Newman, 1987; Guven, 1992; Marry et al., 2008; Johnston, 2010, 2017). A comprehensive review of smectite–water interactions at the molecular level is beyond the scope of this chapter; rather, a framework for understanding these interactions will be introduced by categorising studies as molecular probe or reporter group studies (Johnston et al., 1993; Zecchina and Arean, 1996; Johnston, 2010, 2017). Both molecular probe and reporter group studies rely on one or more 'diagnostic properties' that are sensitive to changes in their local environment. Molecular probes are molecules that are used to interrogate a surface (e.g. H_2O), whereas reporter groups are part of the crystal structure of the clay minerals itself (e.g. structural OH group of a clay mineral). For example, consider the ^2H NMR

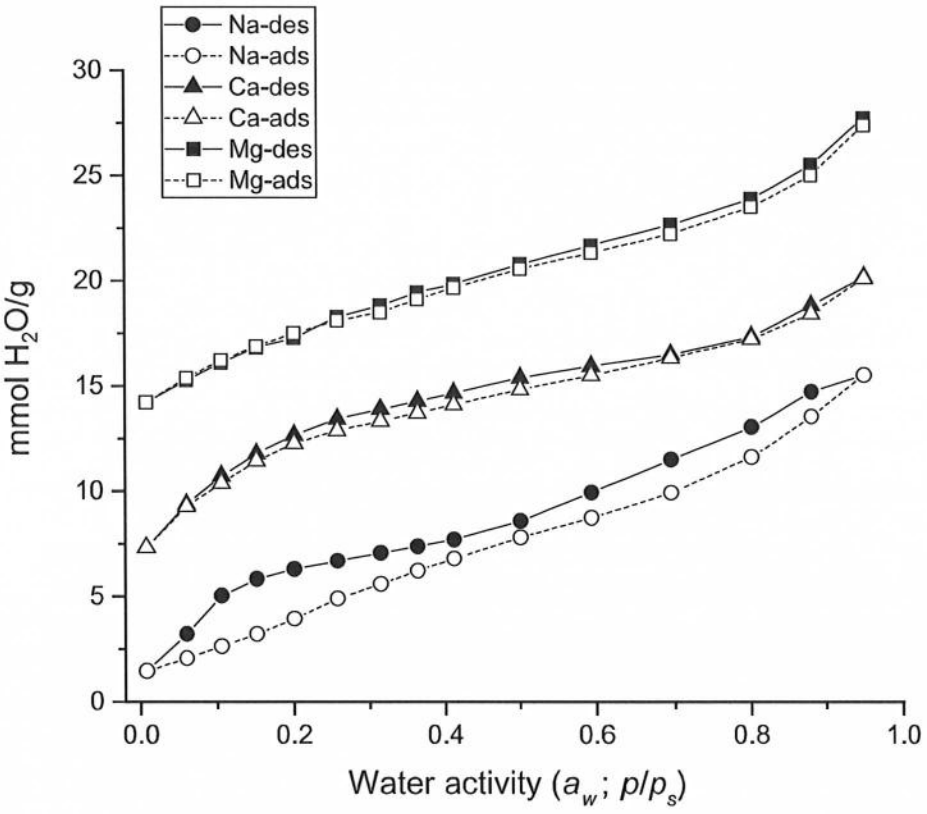

Fig. 4.13 Water desorption and adsorption isotherms of Na^+, Ca^{2+} and Mg^{2+} SAz-1 montmorillonite.
Data were used with permission Xu, W., Johnston, C.T., Parker, P., Agnew, S.F., 2000. Infrared study of water sorption on Na-, Li-, Ca- and Mg-exchanged (SWy-1 and SAz-1) montmorillonite. Clays Clay Miner. 48, 120-131.

behaviour of ^2H_2O (i.e. deuterium oxide or deuterated water). In this case, the quadrupolar coupling constant (QCC) is the diagnostic property of interest that changes with experimental conditions, and ^2H_2O functions as a molecular probe because it can be introduced or removed from the surface. In clay mineral studies, the QCC of ^2H_2O of bulk water (^2H_2O) can be compared to QCC of interlayer water as a function of temperature, water content, and exchangeable cation (Reddy et al., 2016). An ever-expanding group of diagnostic properties are being reported for clay mineral–water interactions that can be observed using vibrational, NMR, EPR, neutron scattering, X-reflectivity, and dielectric relaxation. A partial listing of NMR and vibrational molecular probes and reported groups is illustrated in Fig. 4.14.

Characterisation of smectite–water interactions is strongly dependent on the water activity, nature of the exchangeable cation, clay mineral properties, and environmental variables (e.g. temperature and pressure). Thus, it is important to establish a clear connection between the spectroscopic/structural information with these variables (e.g. water activity, temperature, pressure). This can be achieved using in situ methods that combine techniques such as XRD, IR, or NMR spectroscopy, with methods that can quantify water adsorption (e.g. quartz crystal microbalance). Recent examples of

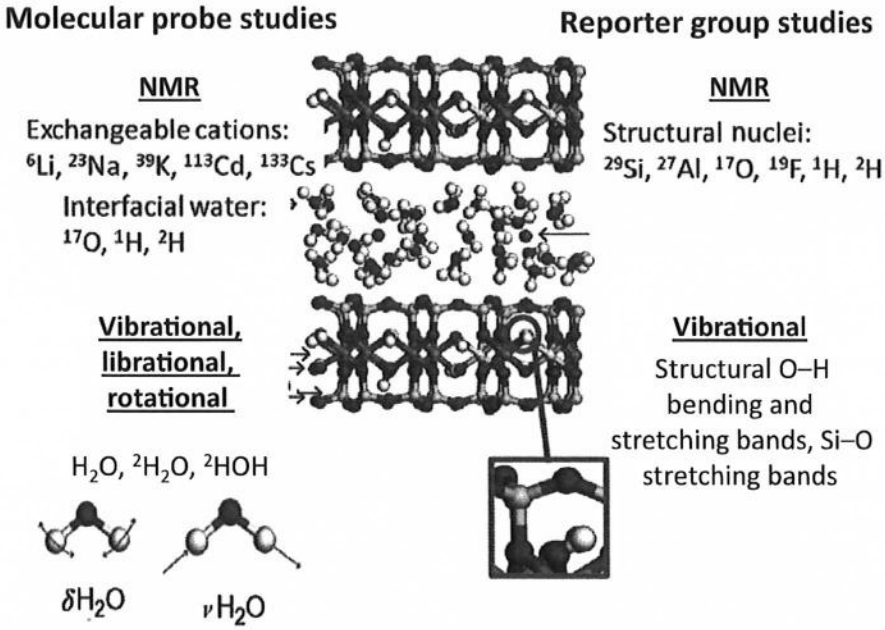

Fig. 4.14 Common molecular probes and reporter groups used to study clay-water interactions.

in situ studies include IR (Schuttlefield et al., 2007a,b; Loring et al., 2014; Thompson et al., 2014; Tang et al., 2016; Schnetzer et al., 2017), NMR (Bowers et al., 2014a,b; Kirkpatrick et al., 2015; Reddy et al., 2016), and XRD (Schaef et al., 2015, 2017). In situ studies provide a direct connection between the points, or a clearly defined region, on the water adsorption isotherm to the structural/spectroscopic properties of interest. A good example is the recent study of Schnetzer et al. (2017) where the concomitant shifts in the vibrational frequency of the H_2O bending band and the structural OH bending bands could be quantitatively related to the number of H_2O molecules coordinated to the interlayer Na^+ ions (Fig. 4.15).

4.4.1 Vibrational studies of smectite–water interactions

The vibrational properties of smectite–water interactions have been used in both molecular probe and reporter group studies (Johnston, 2010, 2017). Water is an ideal molecular probe, as its vibrational modes are sensitive to short-range interactions. In smectite–water studies, the stretching, bending, and librational vibrational modes of H_2O (and ^{2}HOH and $^{2}H_2O$) have been used to study both ion–dipole and hydrogen-bonding interactions (Russell and Farmer, 1964; Poinsignon et al., 1978; Johnston et al., 1992; Xu et al., 2000; Johnston and Premachandra, 2001; Madejova et al., 2002; Dontsova et al., 2004; Schuttlefield et al., 2007b; Kuligiewicz et al., 2015a, b; Schnetzer et al., 2016; Tang et al., 2016; Kuligiewicz and Derkowski, 2017). Vibrational studies have shown that the water molecules clustered around the exchangeable cations are strongly polarised by the cation. The remaining water molecules have similar vibrational properties to those of bulk water. Interestingly, water molecules coordinated to cations in clay mineral interlayers at low water content are less hydrogen

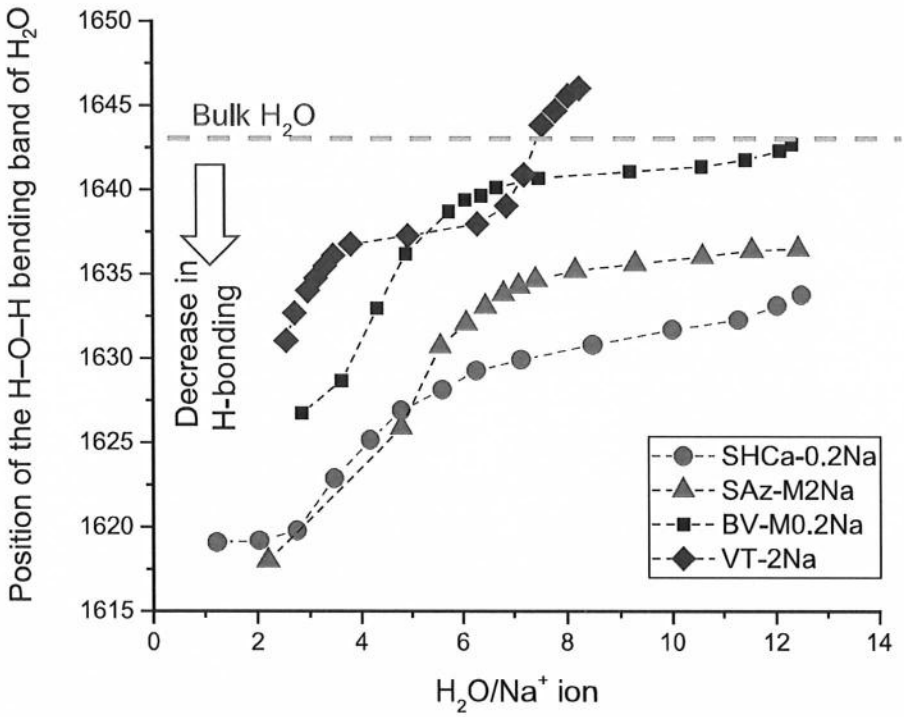

Fig. 4.15 Position of the H–O–H bending band of H_2O as a function of water content expressed as the number of water molecules per Na^+ ion for hectorite (SHCa), two montmorillonite samples (SAz-1 Cheto montmorillonite, and Volclay), and vermiculite (VT).
Data were used with permission from Schnetzer, F., Johnston, C.T., Premachandra, G.S., Giraudo, N., Schuhmann, R., Thissen, P., Emmerich, K., 2017. Impact of intrinsic structural properties on the hydration of 2:1 layer silicates. ACS Earth Space Chem. 1, 608–620.

bonded than in bulk water. Evidence comes from in situ FTIR studies of H_2O adsorbed to different smectites where the shift in the H–O–H bending band of water reflects the overall extent of hydrogen bonding between water molecules (Xu et al., 2000; Schnetzer et al., 2017). A shift of the H–O–H bending band to lower frequencies compared with bulk water indicates an overall decrease in hydrogen bonding (Fig. 4.15). For example, the position of the H–O–H bending band of water in the IR spectra of matrix-isolated or gas phase H_2O is 1594–1597 cm^{-1} and that of liquid H_2O is 1644 cm^{-1} (Venyaminov and Prendergast, 1997). Depending on the water content of the clay, the H–O–H bending can range from ~1647 cm^{-1} at high water content to values <1620 cm^{-1} at low water content (Schnetzer et al., 2017), corresponding to increased and decreased hydrogen bonding, respectively. In addition, the ν(OH) band of adsorbed ^2H_2O and ^2HOH has been used as a probe of smectite surface properties (e.g. charge density) (Kuligiewicz et al., 2015a,b; Szczerba et al., 2016; Kuligiewicz and Derkowski, 2017).

In addition to water, the vibrational features of the clay mineral structure itself provide a type of reporter group. In some cases, these bands (e.g. the structural O—H bending or deformation bands) are sensitive to the presence of water molecules in the interlayer space. Examples of reporter group vibrational studies include (Sposito et al., 1983; Johnston et al., 1992; Xu et al., 2000; Schnetzer et al., 2017).

The structural OH deformation bands, in particular, are sensitive to both the nature of the exchangeable cation and to changes in water content (Xu et al., 2000; Schnetzer et al., 2017).

4.4.2 NMR and EPR studies of smectite–water interactions

NMR spectroscopy provides a comprehensive suite of both molecular probes and reporter groups for studying clay mineral–water interactions (Fig. 4.14). Advantages of NMR spectroscopy for clay mineral–water studies include access to element specific probes, sensitive to both local structure and dynamics over a wide range of timescales from milli- to nanoseconds, and the ability to study longer-range interactions (Kirkpatrick et al., 2015). NMR molecular probes include water (nuclei = ^{2}H, ^{1}H and ^{17}O) (Reddy et al., 2016) and exchangeable cations (e.g. $^{7}Li^{+}$, $^{23}Na^{+}$, $^{39}K^{+}$, $^{43}Ca^{2+}$, $^{87}Sr^{2+}$, $^{113}Cd^{2+}$, $^{133}Cs^{+}$) (Bank et al., 1989; Laperche et al., 1990; Weiss et al., 1990; Alba et al., 1998; Bowers et al., 2014a; Steudel et al., 2015). Structural nuclei used as reporter groups include ^{1}H, ^{2}H, ^{17}O, ^{19}F, ^{27}Al, and ^{29}Si (Sanz et al., 2015; Steudel et al., 2015). Some of these molecular probe and reporter group nuclei are shown in Fig. 4.14. NMR methods can be used to study the coordination and mobility of exchangeable cations, the residence time of interlayer H_2O molecules bonding to other interlayer H_2O molecules, or the residence time of interlayer water bonding to an exchangeable cation (Reddy et al., 2016). Because H_2O in nanoconfined geometries 'freezes' at lower temperatures than in bulk H_2O (e.g. approx. −40°C for Hal), controlled temperature NMR methods are useful to study the transition of liquid H_2O to ice-like structures (Bowers et al., 2014b). The concept of 'freezing' becomes less relevant as water content decreases to values of <10 H_2O molecules per exchangeable cation. In addition, NMR methods can measure longer-range interactions of interest in the mesoscale (2–50 nm, Schoonheydt and Bergaya, 2011) through T_1 and T_2 relaxation rates at timescales extending from frequencies of >1 GHz to <1 kHz (Kirkpatrick et al., 2015). Because these frequencies are much lower than those of vibrational frequencies (THz to PHz), complementary information is obtained using the two methods. The presence of Fe or other paramagnetic impurities strongly interfere with NMR measurements, restricting NMR to clay minerals containing little or no paramagnetic impurities.

Similar to the use of NMR methods, which look at nuclear spin transitions, electron paramagnetic resonance (also known at electron spin resonance, EPR, or ESR) measures electron spin transitions. Similar to NMR, EPR methods have been used to study cationic molecular probes (Cu^{2+}, Fe^{3+}, Mn^{2+}, Cr^{3+}, VO^{2+}) and structural nuclei (Fe^{3+} and Mn^{2+}). EPR spectra of self-supporting clay mineral films oriented parallel and perpendicular to the applied magnetic field provided the first detailed studies of hydrated cation orientation in the interlayer spaces (McBride et al., 1975a,b). In addition, the spin probes (e.g. Cu^{2+} and Fe^{3+}) were used to study single-electron transfer reactions of aromatic hydrocarbons in the interlayer spaces that occurred at low water content. EPR measurements showed both the loss of the spin-probe signal (signifying the metal cation was reduced) and the concomitant formation of a free radical from the organic species (Mortland and Pinnavaia, 1971; Pinnavaia and Mortland, 1971; Fenn et al., 1973; Johnston et al., 1991; Hinedi et al., 1993).

4.4.3 Inelastic and quasielastic neutron scattering of smectite–water interactions

Neutron scattering methods have contributed to the understanding of clay mineral–water interactions for more than four decades (Olejnik et al., 1970; Hunter et al., 1971; Johnston et al., 2000; Bordallo et al., 2008; Martins et al., 2014; Cygan et al., 2015; Jimenez-Ruiz et al., 2017). One of the unique attributes of neutron scattering methods is that these methods are particularly sensitive to the motions of hydrogen atoms. Inelastic neutron scattering (INS) of clay mineral–water interactions in the mid-infrared region can be compared directly with other vibrational spectroscopies, and the spectra can be calculated using molecular simulation (Johnston et al., 2000; Ockwig et al., 2009; Cygan et al., 2015; Jimenez-Ruiz et al., 2017). Similar to earlier EPR and IR studies, oriented clay mineral films can be used to obtain polarisation and orientation information (Michot et al., 2016; Jimenez-Ruiz et al., 2017). Furthermore, advanced molecular simulation methods, such as ab initio molecular dynamics, molecular dynamics (MD), and density functional theory, are now able to simulate the INS spectra at different levels of approximation, and this is an exciting area where experiment and theory can be meaningfully combined (Cygan et al., 2015; Jimenez-Ruiz et al., 2017). The ability to both measure and model water dynamics in confined geometries at geologically relevant temperature and pressures has immediate relevance (Cygan et al., 2015).

In comparison with INS, quasielastic neutron scattering (QENS) examines small energy transfer compared with the incident energy of the scattered particles between neutrons and the sample on 'both sides' (i.e. Stokes and anti-Stokes) of the elastic line (i.e. the energy of incident neutrons). The main contributions to QENS come from the translational and rotational motions of H_2O molecules that have characteristic timescales of 10^{-9}–10^{-10} s, and 10^{-11}–10^{-12} s, respectively (Martins et al., 2014). Early studies compared the self-diffusion coefficient of water (2.14×10^{-9} m^2/s) to that of interlayer H_2O and showed that diffusion of H_2O was significantly hindered by the clay mineral ($0.6–2.5 \times 10^{-10}$ m^2/s) depending on the type of clay mineral (vermiculite or Mt), exchangeable cation and overall water content (Olejnik et al., 1970; Hunter et al., 1971; Cebula et al., 1981). Additional insight was provided by Swenson et al. (2000) in a QENS study of oriented one-H_2O and two-H_2O layer vermiculites. For a two-H_2O layer vermiculite, the translational diffusion of water was about two to three times slower than that of bulk H_2O. More recently, QENS data were combined with molecular simulations to study both the parallel and perpendicular translations of H_2O in a synthetic fluoro-hectorite where the perpendicular component was found to be nonnegligible. In this case, the contribution from structural OH groups was eliminated by replacing OH^- with F^- (Marry et al., 2013). This method has been further extended by combining in situ XRD and QENS with controlled relative humidity (Gates et al., 2017). These authors provided molecular insight about the dynamics of H_2O associated with clay mineral hysteresis and clay mineral dehydration (Gates et al., 2017). In a related study of H_2O in Mt and Hal, the self-diffusion coefficient, average residence time between jumps (τ_o) on interlayer-intercalated H_2O molecules were compared with bulk water and 'surface water.' For both Hal and Mt, the self-diffusion

coefficient of interlayer H_2O molecules was about three times slower than that of bulk water, the average residence time between jumps (τ_o) was 5 to 16 ps compared with 1.5 ps for bulk water (Bordallo et al., 2008).

4.4.4 Dielectric relaxation spectroscopy

Dielectric relaxation spectroscopy (DRS) measures the interaction of a sample with an oscillating electric field. The field-induced polarisation can be measured in the time domain or as a function of the field frequency (Buchner and Hefter, 2009). Compared with other methods, the range of timescales is quite large, extending from far-IR transitions (femtoseconds) to relaxation processes that can take hours (Schmuttenmaer, 2004). In the case of clay mineral–water interactions, DRS is sensitive to a wide range of dynamical processes involving water (Calvet, 1975; Rotenberg et al., 2005; Cadene et al., 2006; Rahman et al., 2015). Different relaxation processes occur over the wide range of timescales, and one of the challenges of DRS is to derive clear mechanistic insight from these processes. In a study of smectite–water interactions, five distinct relaxations were observed, ranging in frequency from 3 kHz to 3 GHz (Cadene et al., 2006). In order to resolve these features, spectral deconvolution methods are required, which can introduce some ambiguity. Of particular interest are the DRS-derived mobilities of the exchangeable cations that can be compared with MD results (Rotenberg et al., 2005). In the terahertz frequency range (also known as far-IR), the librational motions of water, cations, and related species can be resolved (Diaz et al., 2000, 2002a,b; Zich et al., 2013).

4.5 Probing the hydrophobic/hydrophilic character of clay mineral surfaces

The interaction of water with clay mineral surfaces provides important information about the overall hydrophilic character of clay minerals. Although 'wettability' of well-defined macroscopic surfaces can easily be measured by traditional methods (e.g. advancing contact angles), these methods are irrelevant for submicron-sized clay mineral particles due to surface roughness, and contribution of basal vs edge sites. Water adsorption, molecular spectroscopy, structural and imaging methods, and molecular simulation of water on clay mineral surfaces continue to provide mechanistic insight about the fundamental interactions in clay mineral–water systems.

In addition, however, adsorption of organic molecules on clay mineral surfaces provides complementary insight about the overall hydrophobic/hydrophilic nature of a particular surface, and three prototypical examples are given here as examples of hydrophobic/semipolar probes. First, consider the case of metal-uncharged ligand complexes, where in the case of the bis-Cu^{2+}-ethylenediamine complex ($Cu(en)_2^{2+}$), the overall stability constant of this complex exceeds the bulk solution value by three orders of magnitude (Maes et al., 1978; Maes and Cremers, 1979, 1981; Maes et al., 1980). In subsequent spectroscopic work, the authors concluded that the interlayer

space of clay minerals behaves as a 'rigid, anionic solvent' towards $Cu(en)_2^{2+}$ and stabilised the complex. $[Cu(en)_2(H_2O)_2]^{2+}$ loses its two axially coordinated water molecules in the interlayer space. The clay mineral surface acts then as axial ligands, which are much weaker than water (Maes et al., 1980). The second example is from an important study that examined the adsorption of atrazine, a weak organic base, with a range of 14 Ca-exchanged smectites from aqueous solution. Adsorption ranged from essentially complete removal (Freundlich adsorption coefficient (K_f) >1300 for a beidellite), to essentially no adsorption ($K_f = 0.01$) for Otay Mt (Laird et al., 1992). What is interesting from this study was that adsorption varied by three orders of magnitude, but all of the adsorbents were Ca-smectites. Adsorption was related to differences in IHS and surface charge density effects. Based on Laird's work, a number of related compounds, including nitroaromatics and carbamates, have been investigated (Boyd et al., 2011). The last example is from a combined adsorption and spectroscopic study of a strongly hydrophobic compound, dibenzo-*p*-dioxin, with smectites exchanged with different exchangeable cations. In general, one would expect that smectites, which are considered to function as hydrophilic materials, would have little, if any, affinity for dibenzo-*p*-dioxin. For strongly hydrated monovalent and divalent cations, this is indeed the case. However, when the exchangeable cations are K^+ and especially Cs^+, surprisingly high adsorption is observed, and the overall amount of adsorbed dioxin is 10,000 mg/kg (1 wt%) (Liu et al., 2009, 2012; Rana et al., 2009). These studies show that clay mineral surfaces play an important role in stabilising organic compounds; however, a comprehensive understanding about how clay mineral surfaces interact with both H_2O and organic molecules is not yet well understood.

4.6 Conclusions

Because clay minerals are the most abundant nanoparticles and water is the only abundant inorganic liquid on Earth, it follows that clay mineral–water interactions are central to *many* important chemical, physical, or biological process in the biosphere (Robertson, 1986; Hochella et al., 2008). In soil and subsurface environments, the behaviour of water near the surfaces of clay minerals plays essential roles in regulation of most of the interactions occurring in the 'critical zone' (Brantley et al., 2007; Lin, 2010). The world is increasingly dependent upon hydrocarbon recovery from shale oil and gas reservoirs, the energy-water nexus, where clay mineral-water interactions control flow through porous media. As materials, clay minerals are continually finding new applications in materials science and clay-polymer nanocomposites.

Water is intimately associated with the structures of many clay minerals, and is an integral structural component for a number of clay minerals. From a mechanistic perspective, many clay minerals (and their counterions) interact strongly with interfacial water molecules through ion–dipole, hydrogen bonding, and related dipole–dipole interactions. For these clay minerals, the properties of interfacial water are strongly influenced by the surface. For example, the basal siloxane surface of clay minerals can be both hydrophobic in the absence of IHS, or hydrophilic, depending on the extent of charge substitution and the nature of the exchangeable cation. In reality, both

hydrophobic and hydrophilic sites are present on a given clay mineral. In the case of smectites, the overall hydrophobic/hydrophilic character of clay mineral can be controlled through ion exchange of cations with large or small enthalpies of hydration. Even when water molecules are excluded from hydrophobic clay mineral surfaces, these clay minerals play an important role in stabilising organic species. For clay minerals that possess an exposed aluminium or magnesium octahedral sheet surface (e.g. kaolin group minerals), these surfaces are hydrophilic where adhesion (water–surface) interactions are greater than cohesion (water–water) interactions. Kaolinite is an interesting example because it possesses both a hydrophobic siloxane surface and a hydrophilic aluminium hydroxyl surface. After many years of studying clay mineral–water interactions, a broad spectrum of experimental and theoretical insights has been achieved. The great majority of these relate to 'short range' molecular interactions that occur at distances from 0 to 2 nm. As increasingly powerful experimental methods are combined with more sophisticated and powerful molecular simulation methods capable of simulating larger numbers of atoms and electrons, it will be exciting to see how clay mineral-water interaction governs interfacial behaviour at progressively larger scales of >2 nm.

References

Adamo, P., Violante, P., Wilson, M.J., 2001. Tubular and spheroidal halloysite in pyroclastic deposits in the area of the Roccamonfina volcano (Southern Italy). Geoderma 99, 295–316.

Alba, M.D., Alvero, R., Becerro, A.I., Castro, M.A., Trillo, J.M., 1998. Chemical behavior of lithium ions in reexpanded Li-montmorillonites. J. Phys. Chem. B 102, 2207–2213.

Ambers, C.P., Murray, H.H., 1995. The role of carbonate bedrock in the formation of Indianaite halloysitic clays. Indiana Geol. Survey Bull. 65, 1–29.

Auer, B.M., Skinner, J.L., 2008. IR and Raman spectra of liquid water: theory and interpretation. J. Chem. Phys. 128, 12.

Auer, B., Kumar, R., Schmidt, J.R., Skinner, J.L., 2007. Hydrogen bonding and Raman, IR, and 2D-IR spectroscopy of dilute HOD in liquid D2O. Proc. Natl. Acad. Sci. U.S.A. 104, 14215–14220.

Bank, S., Bank, J.F., Ellis, P.D., 1989. Solid-state 113Cd nuclear magnetic resonance study of exchanged montmorillonites. J. Phys. Chem. 93, 4847–4855.

Berend, I., Cases, J.-M., Francois, M., Uriot, J.P., Michot, L., Masion, A., Thomas, F., 1996. Mechanism of adsorption and desorption of water vapor by homoionic montmorillonites: 2. The Li^+ Na^+, K^+, Rb^+ and Cs^+-exchanged forms. Clays Clay Miner. 43, 324–336.

Bergaya, F., Lagaly, G. (Eds.), 2013a. Handbook of Clay Science. Part A: Fundamentals. second ed. Elsevier, Amsterdam, NL.

Bergaya, F., Lagaly, G. (Eds.), 2013b. Handbook of Clay Science. Part B: Techniques and Applications. second ed. Elsevier, Amsterdam, NL.

Bordallo, H.N., Aldridge, L.P., Churchman, G.J., Gates, W.P., Telling, M.T.F., Kiefer, K., Fouquet, P., Seydel, T., Kimber, S.a.J., 2008. Quasi-elastic neutron scattering studies on clay interlayer-space highlighting the effect of the cation in confined water dynamics. J. Phys. Chem. C 112, 13982–13991.

Bowers, G.M., Hoyt, D.W., Burton, S.D., Ferguson, B.O., Varga, T., Kirkpatrick, R.J., 2014a. In situ C^{-13} and Na^{-23} magic angle spinning NMR investigation of supercritical CO_2 incorporation in smectite-natural organic matter composites. J. Phys. Chem. C 118, 3564–3573.

Bowers, G.M., Singer, J.W., Bish, D.L., Kirk patrick, J., 2014b. Structural and dynamical relationships of Ca^{2+} and H_2O in smectite/$(H_2O)^{-}H^{-2}$ systems. Am. Mineral. 99, 318–331.

Boyd, S.A., Johnston, C.T., Laird, D.A., Teppen, B.J., Li, H., 2011. Comprehensive study of organic contaminant adsorption by clays: methodologies, mechanisms, and environmental implications. In: Xing, B., Senesi, N., Huang, P.M. (Eds.), Biophysico-Chemical Processes of Anthropogenic Organic Compounds in Environmental Systems. John Wiley & Sons, Inc.

Brantley, S.L., Goldhaber, M.B., Ragnarsdottir, K.V., 2007. Crossing disciplines and scales to understand the critical zone. Elements 3, 307–314.

Brigatti, M.F., Galán, E., Theng, B.K.G., 2013. Chapter 2—structure and mineralogy of clay minerals. In: Bergaya, F., Lagaly, G. (Eds.), Developments in Clay Science. Elsevier.

Buchner, R., Hefter, G., 2009. Interactions and dynamics in electrolyte solutions by dielectric spectroscopy. Phys. Chem. Chem. Phys. 11, 8984–8999.

Burgess, J., 1999. 4—Ion–Solvent Interactions. Ions in Solution, second ed. Woodhead Publishing.

Cadene, A., Rotenberg, B., Durand-Vidal, S., Badot, J.C., Turq, P., 2006. Dielectric spectroscopy as a probe for dynamic properties of compacted smectites. Phys. Chem. Earth 31, 505–510.

Calvet, R., 1975. Dielectric properties of montmorillonites saturated by bivalent cations. Clays Clay Miner. 23, 257–265.

Cancela, G.D., Huertas, F.J., Taboada, E.R., Sanchezrasero, F., Laguna, A.H., 1997. Adsorption of water vapor by homoionic montmorillonites. Heats of adsorption and desorption. J. Colloid Interface Sci. 185, 343–354.

Cases, J.M., Berend, I., Besson, G., Francois, M., Uriot, J.P., Thomas, F., Poirier, J.E., 1992. Mechanism of adsorption and desorption of water vapor by homoionic montmorillonite. 1. The sodium-exchanged form. Langmuir 8, 2730–2739.

Cases, J.M., Berend, I., Francois, M., Uriot, J.P., Michot, L.J., Thomas, F., 1997. Mechanism of adsorption and desorption of water vapor by homoionic montmorillonite. 3. The Mg^{2+}, Ca^{2+}, Sr^{2+} and Ba^{2+} exchanged forms. Clays Clay Miner. 45, 8–22.

Cebula, D.J., Thomas, R.K., White, J.W., 1981. Diffusion of water in Li-montmorillonite studied by quasielastic neutron scattering. Clays Clay Miner. 29, 241–248.

Chinnery, N.J., Pawley, A.R., Clark, S.M., 1999. In situ observation of the formation of 10 angstrom phase from talc plus H_2O at mantle pressures and temperatures. Science 286, 940–942.

Coblentz, W.W., 1910. Note on water of crystallization. Phys. Rev. 30, 322–327.

Coblentz, W.W., 1911. The role of water in minerals. J. Franklin Inst. 172, 309–335.

Collins, K.D., 1997. Charge density-dependent strength of hydration and biological structure. Biophys. J. 72, 65–76.

Collins, K.D., 2004. Ions from the Hofmeister series and osmolytes: effects on proteins in solution and in the crystallization process. Methods 34, 300–311.

Collins, K.D., Neilson, G.W., Enderby, J.E., 2007. Ions in water: characterizing the forces that control chemical processes and biological structure. Biophys. Chem. 128, 95–104.

Costanzo, P.M., Guggenheim, S., 2001. Baseline studies of the clay minerals society source clays. Clays Clay Miner. 49, 371–452.

Cruz, M.I., Letellier, M., Fripiat, J.J., 1978. NMR study of adsorbed water. II. Molecular motions in the monolayer hydrate of halloysite. J. Chem. Phys. 69, 2018–2027.

Cuadros, J., Dudek, T., 2006. FTIR investigation of the evolution of the octahedral sheet of kaolinite-smectite with progressive kaolinization. Clays Clay Miner. 54, 1–11.

Cygan, R.T., Daemen, L.L., Ilgen, A.G., Krumhansl, J.L., Nenoff, T.M., 2015. Inelastic neutron scattering and molecular simulation of the dynamics of inter layer water in smectite clay minerals. J. Phys. Chem. C 119, 28005–28019.

Debenedetti, P.G., 2003. Supercooled and glassy water. J. Phys. Condens. Matter 15, R1669–R1726.

Derjaguin, B., Landau, L., 1941. Theory of the stability of strongly charged lyophobic sols and of the adhesion of strongly charged particles in solutions of electrolytes. Acta Physicochim. URSS 14, 633.

Dewalt-Kerian, E.L., Kim, S., Azam, M.S., Zeng, H.B., Liu, Q.X., Gibbs, J.M., 2017. pH-dependent inversion of Hofmeister trends in the water structure of the electrical double layer. J. Phys. Chem. Lett. 8, 2855–2861.

Diaz, M., Farmer, V.C., Prost, R., 2000. Characterization and assignment of far infrared absorption bands of K^+ in muscovite. Clays Clay Miner. 48, 433–438.

Diaz, M., Huard, E., Prost, R., 2002a. Far infrared analysis of the structural environment of interlayer K^+, NH_4^+, Rb^+ and Cs^+ selectively retained by vermiculite. Clays Clay Miner. 50, 284–293.

Diaz, M., Laperche, V., Harsh, J., Prost, R., 2002b. Far infrared spectra of K^+ in dioctahedral and trioctahedral mixed-layer minerals. Am. Mineral. 87, 1207–1214.

Dontsova, K.M., Norton, L.D., Johnston, C.T., Bigham, J.M., 2004. Influence of exchangeable cation on water adsorption by soil clays. Soil Sci. Soc. Am. J. 68, 1218–1227.

Douillard, J.M., Medout-Marere, V., 2000. Surface Energy and Acid-Base Properties of Solids Studied by Immersion Calorimetry. Vsp Bv-C/O Brill Academic Publishers, Leiden.

Douillard, J.M., Malandrini, H., Zoungrana, T., Clauss, F., Partyka, S., 1994. Surface-tension of talc and talc-chlorite mixtures. J. Thermal Anal. 41, 1205–1210.

Douillard, J.M., Zajac, J., Malandrini, H., Clauss, F., 2002. Contact angle and film pressure: study of a talc surface. J. Colloid Interface Sci. 255, 341–351.

Du, Q., Freysz, E., Shen, Y.R., 1994. Vibrational spectra of water molecules at quartz-water interfaces. Phys. Rev. Let. 72, 238–241.

Emmerich, K., 2013. Chapter 2.13—full characterization of smectites. In: Bergaya, F., Lagaly, G. (Eds.), Developments in Clay Science. Elsevier.

Fenn, D.B., Mortland, M.M., Pinnavaia, T.J., 1973. The chemisorption of anisole on Cu(II)-hectorite. Clays Clay Miner. 21, 315–322.

Ferrante, F., Armata, N., Lazzara, G., 2015. Modeling of the halloysite spiral nanotube. J. Phys. Chem. C 119, 16700–16707.

Fialips, C.I., Petit, S., Decarreau, A., 2000. Hydrothermal formation of kaolinite from various metakaolins. Clay Miner. 35, 559–572.

Fraser, H.J., Mccoustra, M.R.S., Williams, D.A., 2002. The molecular universe. Astron. Geophys. 43, 10–18.

Frost, R.L., 1995. Fourier transform Raman spectroscopy of kaolinite, dickite and halloysite. Clays Clay Miner. 43, 191–195.

Frost, R.L., Kristof, J., 1997. Intercalation of halloysite: a Raman spectroscopic study. Clays Clay Miner. 45, 551–563.

Frost, R.L., Shurvell, H.F., 1997. Raman microprobe spectroscopy of halloysite. Clays Clay Miner. 45, 68–72.

Gallo, P., Arnann-Winkel, K., Angell, C.A., Anisimov, M.A., Caupin, F., Chakravarty, C., Lascaris, E., Loerting, T., Panagiotopoulos, A.Z., Russo, J., Sellberg, J.A., Stanley, H.E., Tanaka, H., Vega, C., Xu, L.M., Pettersson, L.G.M., 2016. Water: a tale of two liquids. Chem. Rev. 116, 7463–7500.

Gates, W.P., Aldridge, L.P., Carnero-Guzman, G.G., Mole, R.A., Yu, D.H., Iles, G.N., Klapproth, A., Bordallo, H.N., 2017. Water desorption and absorption isotherms of sodium montmorillonite: a QENS study. Appl. Clay Sci. 147, 97–104.

Giese, K., Kaatze, U., Pottel, R., 1970. Permittivity and dielectric and proton magnetic relaxation of aqueous solutions of alkali halides. J. Phys. Chem. 74, 3718.

Giese, R.F., Costanzo, P.M., Vanoss, C.J., 1991. The surface free energies of talc and pyrophyllite. Phys. Chem. Miner. 17, 611–616.

Gilbert, B., Comolli, L.R., Tinnacher, R.M., Kunz, M., Banfield, J.F., 2015. Formation and restacking of disordered smectite osmotic hydrates. Clays Clay Miner. 63, 432–442.

Götte, L., Parry, K.M., Hua, W., Verreault, D., Allen, H.C., Tobias, D.J., 2017. Solvent-shared ion pairs at the air–solution interface of magnesium chloride and sulfate solutions revealed by sum frequency spectroscopy and molecular dynamics simulations. J. Phys. Chem. A 121, 6450–6459.

Guven, N., 1992. Molecular aspects of clay/water interactions. In: Guven, N., Pollastro, R.M. (Eds.), Clay-Water Interface and Its Rheological Implications. The Clay Minerals Society, Boulder, CO.

Hall, P.L., Astill, D.M., 1989. Adsorption of water by homoionic exchange forms of Wyoming montmorillonite (SWy-1). Clays Clay Miner. 37, 355–363.

Hazen, R.M., Ferry, J.M., 2010. Mineral evolution: mineralogy in the fourth dimension. Elements 6, 9–12.

Hinedi, Z.R., Johnston, C.T., Erickson, C., 1993. Chemisorption of benzene on Cu-montmorillonite as characterized by FTIR and ^{13}C MAS NMR. Clays Clay Miner. 41, 87–94.

Hirsemann, D., Shylesh, S., De Souza, R.A., Diar-Bakerly, B., Biersack, B., Mueller, D.N., Martin, M., Schobert, R., Breu, J., 2012. Large-scale, low-cost fabrication of Janus-type emulsifiers by selective decoration of natural kaolinite platelets. Angew. Chem. Int. Ed. 51, 1348–1352.

Hochella, M.F., Lower, S.K., Maurice, P.A., Penn, R.L., Sahai, N., Sparks, D.L., Twining, B.S., 2008. Nanominerals, mineral nanoparticles, and Earth systems. Science 319, 1631–1635.

Hu, X.L., Michaelides, A., 2010. The kaolinite (001) polar basal plane. Surf. Sci. 604, 111–117.

Hua, W., Verreault, D., Huang, Z.S., Adams, E.M., Allen, H.C., 2014. Cation effects on interfacial water organization of aqueous chloride solutions. I. Monovalent cations: Li^+, Na^+, K^+, and NH_4^+. J. Phys. Chem. B 118, 8433–8440.

Hunter, R.J., Stirling, G.C., White, J.W., 1971. Water dynamics in clays by neutron spectroscopy. Nat. Phys. Sci. 230, 192.

Janik, L.J., Keeling, J.L., 1993. FT-Ir partial least-squares analysis of tubular halloysite in kaolin samples from the mount hope kaolin deposit. Clay Miner. 28, 365–378.

Jeanmairet, G., Marry, V., Levesque, M., Rotenberg, B., Borgis, D., 2014. Hydration of clays at the molecular scale: the promising perspective of classical density functional theory. Mol. Phys. 112, 1320–1329.

Jimenez-Ruiz, M., Ferrage, E., Blanchard, M., Fernandez-Castanon, J., Delville, A., Johnson, M.R., Michot, L.J., 2017. Combination of inelastic neutron scattering experiments and ab initio quantum calculations for the study of the hydration properties of oriented saponites. J. Phys. Chem. C 121, 5029–5040.

Johnston, C.T., 2010. Probing the nanoscale architecture of clay minerals. Clay Miner. 45, 245–279.

Johnston, C.T., 2017. Infrared studies of clay mineral-water interactions. In: Gates, W.P., Kloprogge, J.T., Madejova, J., Bergaya, F. (Eds.), Infrared and Raman Spectroscopies of Clay Minerals. Elsevier, Amsterdam.

Johnston, C.T., Premachandra, G.S., 2001. Polarized ATR-FTIR study of smectite in aqueous suspension. Langmuir 17, 3712–3718.

Johnston, C.T., Tipton, T., Stone, D.A., Erickson, C., Trabue, S.L., 1991. Chemisorption of p-dimethoxybenzene on Cu-montmorillonite. Langmuir 7, 289–296.

Johnston, C.T., Sposito, G., Erickson, C., 1992. Vibrational probe studies of water interactions with montmorillonite. Clays Clay Miner. 40, 722–730.

Johnston, C.T., Sposito, G., Earl, W.L., 1993. Surface spectroscopy of environmental particles by Fourier transform infrared and nuclear magnetic resonance spectroscopy. In: Buffle, J., Van Leeuwen, H.P. (Eds.), Environmental Particles. In: The Environmental Analytical and Physical Chemistry Series, vol. 2. Lewis Publ, Boca Raton.

Johnston, C.T., Bish, D.L., Eckert, J., Brown, L.A., 2000. Infrared and inelastic neutron scattering study of the 1.03-and 0.95-nm kaolinite-hydrazine intercalation complexes. J. Phys. Chem. B 104, 8080–8088.

Joussein, E., Petit, S., Churchman, J., Theng, B., Righi, D., Delvaux, B., 2005. Halloysite clay minerals—a review. Clay Miner. 40, 383–426.

Keenan, A.G., Mooney, R.W., Wood, L.A., 1951. The relation between exchangeable ions and water adsorption on kaolinite. J. Phys. Colloid Chem. 55, 1462–1474.

Kirillova, A., Stoychev, G., Ionov, L., Eichhorn, K.J., Malanin, M., Synytska, A., 2014. Platelet Janus particles with hairy polymer shells for multifunctional materials. ACS Appl. Mater. Interfaces 6, 13106–13114.

Kirillova, A., Marschelke, C., Friedrichs, J., Werner, C., Synytska, A., 2016. Hybrid hairy Janus particles as building blocks for antibiofouling surfaces. ACS Appl. Mater. Interfaces 8, 32591–32603.

Kirkpatrick, R.J., Kalinichev, A.G., Bowers, G.M., Yazaydin, A.O., Krishnan, M., Saharay, M., Morrow, C.P., 2015. NMR and computational molecular modeling studies of mineral surfaces and interlayer galleries: a review. Am. Mineral. 100, 1341–1354.

Kristof, J., Toth, M., Gabor, M., Szabo, P., Frost, R.L., 1997. Study of the structure and thermal behaviour of intercalated kaolinites. J. Thermal Anal. 49, 1441–1448.

Kuligiewicz, A., Derkowski, A., 2017. Tightly bound water in smectites. Am. Mineral. 102, 1073–1090.

Kuligiewicz, A., Derkowski, A., Emmerich, K., Christidis, G.E., Tsiantos, C., Gionis, V., Chryssikos, G.D., 2015a. Measuring the layer charge of dioctahedral smectite by O-D vibrational spectroscopy. Clays Clay Miner. 63, 443–456.

Kuligiewicz, A., Derkowski, A., Szczerba, M., Gionis, V., Chryssikos, G.D., 2015b. Revisiting the infrared spectrum of the water-smectite interface. Clays Clay Miner. 63, 15–29.

Kumar, N., Zhao, C.L., Klaassen, A., Van Den Ende, D., Mugele, F., Siretanu, I., 2016. Characterization of the surface charge distribution on kaolinite particles using high resolution atomic force microscopy. Geochim. Cosmochim. Acta 175, 100–112.

Laird, D.A., Barriuso, E., Dowdy, R.H., Koskinen, W.C., 1992. Adsorption of atrazine on smectites. Soil Sci. Soc. Am. J. 56, 62–67.

Laperche, V., Lambert, J.F., Prost, R., Fripiat, J.J., 1990. High-resolution solid-state NMR of exchangeable cations in the interlayer surface of a swelling mica: ^{23}NA, ^{111}Cd, and ^{133}Cs vermiculites. J. Phys. Chem. 94, 8821–8831.

Lavikainen, L.P., Tanskanen, J.T., Schatz, T., Kasa, S., Pakkanen, T.A., 2015. Montmorillonite interlayer surface chemistry: effect of magnesium ion substitution on cation adsorption. Theor. Chem. Accounts 134, 7.

Lee, J.H., Guggenheim, S., 1981. Single-crystal X-ray refinement of pyrophyllite-1TC. Am. Mineral. 66, 350–357.

Li, F., Skinner, J.L., 2010a. Infrared and Raman line shapes for ice Ih. I. Dilute HOD in H_2O and D_2O. J. Chem. Phys. 132, 204505.

Li, F., Skinner, J.L., 2010b. Infrared and Raman line shapes for ice Ih. II. H_2O and D_2O. J. Chem. Phys. 133, 244504.

Lin, H., 2010. Earth's critical zone and hydropedology: concepts, characteristics, and advances. Hydrol. Earth Syst. Sci. 14, 25–45.

Liu, C., Li, H., Teppen, B.J., Johnston, C.T., Boyd, S.A., 2009. Mechanisms associated with the high adsorption of dibenzo-p-dioxin from water by smectite clays. Environ. Sci. Technol. 43, 2777–2783.

Liu, C., Li, H., Johnston, C.T., Boyd, S.A., Teppen, B.J., 2012. Relating clay structural factors to dioxin adsorption by smectites: molecular dynamics simulations. Soil Sci. Soc. Am. J. 76, 110–120.

Loring, J.S., Ilton, E.S., Chen, J., Thompson, C.J., Martin, P.F., Benezeth, P., Rosso, K.M., Felmy, A.R., Schaef, H.T., 2014. In situ study of CO_2 and H_2O partitioning between Na-montmorillonite and variably wet supercritical carbon dioxide. Langmuir 30, 6120–6128.

Lvov, Y.M., Shchukin, D.G., Mohwald, H., Price, R.R., 2008. Halloysite clay nanotubes for controlled release of protective agents. ACS Nano 2, 814–820.

Madejova, J., Janek, M., Komadel, P., Herbert, H.J., Moog, H.C., 2002. FTIR analyses of water in MX-80 bentonite compacted from high salinary salt solution systems. Appl. Clay Sci. 20, 255–271.

Maes, A., Cremers, A., 1979. Stability of metal uncharged ligand complexes in ion exchangers. Part 4. Hydration effects and stability changes of copper-ethylenediamine complexes in montmorillonite. J. Chem. Soc. Faraday Trans. 1 75, 513–524.

Maes, A., Cremers, A., 1981. Influence of charge-density on the acid-base-equilibrium of ethylenediamine in montmorillonites. J. Chem. Soc., Faraday Trans.1 77, 1553–1559.

Maes, A., Peigneur, P., Cremers, A., 1978. Stability of metal uncharged ligand complexes in ion exchangers. Part 2.—the copper+ethylenediamiine complex in montmorillonite and sulphonic acid resin. J. Chem. Soc. Faraday Trans. 1 74, 182–189.

Maes, A., Schoonheydt, R.A., Cremers, A., Uytterhoeven, J.B., 1980. Spectroscopy of Cu(en)2 2^+ on clay surfaces. Surface and charge-density effects. J. Phys. Chem. 84, 2795–2799.

Malandrini, H., Clauss, F., Partyka, S., Douillard, J.M., 1997. Interactions between talc particles and water and organic solvents. J. Colloid Interface Sci. 194, 183–193.

Marcus, Y., 1987. The thermodynamics of solvations of ions. 2. The enthalpy of hydration at 298.15 K. J. Chem. Soc., Faraday Trans.1 83, 339–349.

Marcus, Y., 1988. Ionic radii in aqueous-solutions. Chem. Rev. 88, 1475–1498.

Marcus, Y., 2009. Effect of ions on the structure of water: structure making and breaking. Chem. Rev. 109, 1346–1370.

Marcus, Y., 2015a. Ion solvation in neat solvents. In: Ions in Solution and Their Solvation. John Wiley & Sons, Inc.

Marcus, Y., 2015b. Mutual effects of ions and solvents. In: Ions in Solution and Their Solvation. John Wiley & Sons, Inc.

Marry, V., Rotenberg, B., Turq, P., 2008. Structure and dynamics of water at a clay surface from molecular dynamics simulation. Phys. Chem. Chem. Phys. 10, 4802–4813.

Marry, V., Dubois, E., Malikova, N., Breu, J., Haussler, W., 2013. Anisotropy of water dynamics in clays: insights from molecular simulations for experimental QENS analysis. J. Phys. Chem. C 117, 15106–15115.

Martins, M.L., Gates, W.P., Michot, L., Ferrage, E., Marry, V., Bordallo, H.N., 2014. Neutron scattering, a powerful tool to study clay minerals. Appl. Clay Sci. 96, 22–35.

Mcbride, M.B., Pinnavaia, T.J., Mortland, M.M., 1975a. Electron spin relaxation and the mobility of manganese(II) exchange ions in smectites. Am. Mineral. 60, 66–72.

Mcbride, M.B., Pinnavaia, T.J., Mortland, M.M., 1975b. Electron spin resonance studies of cation orientation in restricted water layers on phyllosilicate (smectite) surfaces. J. Phys. Chem. 79, 2430–2435.

Michot, L.J., Villieras, F., Francois, M., Yvon, J., Ledred, R., Cases, J.M., 1994. The structural microscopic hydrophilicity of talc. Langmuir 10, 3765–3773.

Michot, L.J., Ferrage, E., Delville, Jimenez-Ruiz, M. 2016. Influence of layer charge, hydration state and cation nature on the collective dynamics of interlayer water in synthetic swelling clay minerals. Appl. Clay Sci., 119, 375–384.

Mignon, P., Ugliengo, P., Sodupe, M., Hernandez, E.R., 2010. Ab initio molecular dynamics study of the hydration of Li^+, Na^+ and K^+ in a montmorillonite model. Influence of isomorphic substitution. Phys. Chem. Chem. Phys. 12, 688–697.

Mooney, R.W., Keenan, A.G., Wood, L.A., 1952a. Adsorption of water vapor by montmorillonite. I. Heat of desorption and application of BET theory. J. Am. Chem. Soc. 74, 1367–1374.

Mooney, R.W., Keenan, A.G., Wood, L.A., 1952b. Adsorption of water vapor by montmorillonite. II. Effect of exchangeable ions and lattice swelling as measured by X-ray diffraction. J. Am. Chem. Soc. 74, 1371–1374.

Mortland, M.M., Pinnavaia, T.J., 1971. Formation of copper(II) arene complexes on the interlamellar surfaces of montmorillonite. Nature 229, 75–77.

Mottl, M.J., Glazer, B.T., Kaiser, R.I., Meech, K.J., 2007. Water and astrobiology. Chem. Erde-Geochem. 67, 253–282.

Newman, A.C.D., 1987. The interaction of water with clay mineral surfaces. In: Newman, A.C.D. (Ed.), Chemistry of Clays and Clay Minerals. Mineralogical Society, London. Monograph No. 6.

Ni, Y.C., Skinner, J.L., 2015. IR and SFG vibrational spectroscopy of the water bend in the bulk liquid and at the liquid-vapor interface, respectively. J. Chem. Phys. 143, 12.

Norrish, K., 1954. The swelling of montmorillonite. Discuss. Faraday Soc. 18, 120–134.

Ockwig, N.W., Greathouse, J.A., Durkin, J.S., Cygan, R.T., Daemen, L.L., Nenoff, T.M., 2009. Nanoconfined water in magnesium-rich 2:1 phyllosilicates. J. Am. Chem. Soc. 131, 8155–8162.

Ohtaki, H., Radnai, T., 1993. Structure and dynamics of hydrated ions. Chem. Rev. 93, 1157–1204.

Olejnik, S., Stirling, G.C., White, J.W., 1970. Neutron scattering studies of hydrated layer silicates. Spec. Discuss. Faraday Soc. 1, 194–201.

Parry, S.A., Pawley, A.R., Jones, R.L., Clark, S.M., 2007. An infrared spectroscopic study of the OH stretching frequencies of talc and 10-A phase to 10 GPa. Am. Mineral. 92, 525–531.

Partyka, S., Douillard, J.M., 1995. Nature of interactions between organic pure liquids and model rocks—a calorimetric investigation. J. Petrol. Sci. Eng. 13, 95–102.

Pawley, A.R., Welch, M.D., 2014. Further complexities of the 10 angstrom phase revealed by infrared spectroscopy and X-ray diffraction. Am. Mineral. 99, 712–719.

Perakis, F., De Marco, L., Shalit, A., Tang, F.J., Kann, Z.R., Kuhne, T.D., Torre, R., Bonn, M., Nagata, Y., 2016. Vibrational spectroscopy and dynamics of water. Chem. Rev. 116, 7590–7607.

Perdikatsis, B., Burzlaff, H., 1981. Structural refinement of talc $Mg_3(OH)2Si_4O_{10}$. Z. Kristallogr. 156, 177–186.

Pettersson, L.G.M., Henchman, R.H., Nilsson, A., 2016. Water—the most anomalous liquid. Chem. Rev. 116, 7459–7462.

Pinnavaia, T.J., Mortland, M.M., 1971. Interlamellar metal complexes on layer silicates. I. Copper(II)-arene complexes on montmorillonite. J. Phys. Chem. 75 (26), 3957–3962.

Poinsignon, C., Cases, J.M., Fripiat, J.J., 1978. Electrical-polarization of water molecules adsorbed by smectites. An infrared study. J. Phys. Chem. 82, 1855–1860.

Polansky, R., Kadlec, P., Kolska, Z., Svorcik, V., 2017. Influence of dehydration on the dielectric and structural properties of organically modified montmorillonite and halloysite nanotubes. Appl. Clay Sci. 147, 19–27.

Prost, R., Koutit, T., Benchara, A., Huard, E., 1998. State and location of water adsorbed on clay minerals: consequences of the hydration and swelling-shrinkage phenomena. Clays Clay Miner. 46, 117–131.

Rahman, R., Mccarty, D.K., Prasad, M., 2015. Sub-THz complex dielectric constants of smectite clay thin samples with Na+/Ca^{++} ions. J. Geophys. Res. Solid Earth 120, 6219–6225.

Rana, K., Boyd, S.A., Teppen, B.J., Li, H., Liu, C., Johnston, C.T., 2009. Probing the microscopic hydrophobicity of smectite surfaces. A vibrational spectroscopic study of dibenzo-p-dioxin sorption to smectite. Phys. Chem. Chem. Phys. 11, 2976–2985.

Rashchenko, S.V., Likhacheva, A.Y., Goryainov, S.V., Krylov, A.S., Litasov, K.D., 2016. In situ spectroscopic study of water intercalation into talc: new features of 10 angstrom phase formation. Am. Mineral. 101, 431–436.

Reddy, U.V., Bowers, G.M., Loganathan, N., Bowden, M., Yazaydin, A.O., Kirkpatrick, R.J., 2016. Water structure and dynamics in smectites: X-ray diffraction and ^{2}H NMR spectroscopy of Mg–, Ca–, Sr–, Na–, Cs–, and Pb–hectorite. J. Phys. Chem. C 120, 8863–8876.

Robertson, R.H.S., 1986. Fuller's Earth: A History of Calcium Montmorillonite. Volturna Press, Hythe, Kent, UK.

Rotenberg, B., Cadene, A., Dufreche, J.F., Durand-Vidal, S., Badot, J.C., Turq, P., 2005. An analytical model for probing ion dynamics in clays with broadband dielectric spectroscopy. J. Phys. Chem. B 109, 15548–15557.

Rotenberg, B., Patel, A.J., Chandler, D., 2011. Molecular explanation for why talc surfaces can be both hydrophilic and hydrophobic. J. Am. Chem. Soc. 133, 20521–20527.

Russell, J.D., Farmer, V.C., 1964. Infra-red spectroscopic study of the dehydration of montmorillonite and saponite. Clay Miner. Bull. 5, 443–464.

Sanz, J., Sobrados, I., Robert, J.L., 2015. Influence of hydration on Na-23, Al-27, and Si-29 MAS-NMR spectra of sodium saponites and sodium micas. Am. Mineral. 100, 1076–1083.

Schaef, H.T., Loring, J.S., Glezakou, V.A., Miller, Q.R.S., Chen, J., Owen, A.T., Lee, M.S., Ilton, E.S., Felmy, A.R., Mcgrail, B.P., Thompson, C.J., 2015. Competitive sorption of CO2 and H2O in 2:1 layer phyllosilicates. Geochim. Cosmochim. Acta 161, 248–257.

Schaef, H.T., Loganathan, N., Bowers, G.M., Kirkpatrick, R.J., Yazaydin, A.O., Burton, S.D., Hoyt, D.W., Thanthiriwatte, K.S., Dixon, D.A., Mcgrail, B.P., Rosso, K.M., Ilton, E.S., Loring, J.S., 2017. Tipping point for expansion of layered aluminosilicates in weakly polar solvents: supercritical CO2. ACS Appl. Mater. Interfaces 9, 36783–36791.

Schmuttenmaer, C.A., 2004. Exploring dynamics in the far-infrared with terahertz spectroscopy. Chem. Rev. 104, 1759–1779.

Schnetzer, F., Thissen, P., Giraudo, N., Emmerich, K., 2016. Unraveling the coupled processes of (de)hydration and structural changes in Na^{+}-saturated montmorillonite. J. Phys. Chem. C 120, 15282–15287.

Schnetzer, F., Johnston, C.T., Premachandra, G.S., Giraudo, N., Schuhmann, R., Thissen, P., Emmerich, K., 2017. Impact of intrinsic structural properties on the hydration of 2:1 layer silicates. ACS Earth and Space Chem. 1, 608–620.

Schoonheydt, R.A., Bergaya, F., 2011. Industrial clay minerals as nanomaterials, Chapter 10. In: Christidis, G. (Ed.), Advances in the Characterization of Industrial Minerals. EMU Notes in Mineralogy, vol. 9. Miner. Soc. Publishers, pp. 415–440.

Schoonheydt, R.A., Johnston, C.T., 2013. Surface and interface chemistry of clay minerals. In: Bergaya, F., Theng, B.K.G., Lagaly, G. (Eds.), Handbook of Clay Science, second ed. Part A. Fundamentals, Elsevier, Amsterdam.

Schrader, M.E., Yariv, S., 1990. Wettability of clay minerals. J. Colloid Interface Sci. 136, 85–94.

Schuttlefield, J., Al-Hosney, H., Zachariah, A., Grassian, V.H., 2007a. Attenuated total reflection Fourier transform infrared spectroscopy to investigate water uptake and phase transitions in atmospherically relevant particles. Appl. Spectrosc. 61, 283–292.

Schuttlefield, J.D., Cox, D., Grassian, V.H., 2007b. An investigation of water uptake on clays minerals using ATR-FTIR spectroscopy coupled with quartz crystal microbalance measurements. J. Geophys. Res. Atmos. 112, D21303, https://doi.or/10.1029/2007JD008973.

Shang, J.Y., Flury, M., Harsh, J.B., Zollars, R.L., 2010. Contact angles of aluminosilicate clays as affected by relative humidity and exchangeable cations. Colloids Surf. A Physicochem. Eng. Asp. 353, 1–9.

Shchukin, D.G., Sukhorukov, G.B., Price, R.R., Lvov, Y.M., 2005. Halloysite nanotubes as biomimetic nanoreactors. Small 1, 510–513.

Solc, R., Gerzabek, M.H., Lischka, H., Tunega, D., 2011. Wettability of kaolinite (001) surfaces—molecular dynamic study. Geoderma 169, 47–54.

Soper, A.K., Neilson, G.W., Enderby, J.E., Howe, R.A., 1977. Neutron diffraction study of hydration effects in aqueous solutions. J. Phys. C Solid State Phys. 10, 1793–1801.

Sposito, G., Prost, R., 1982. Structure of water adsorbed on smectites. Chem. Rev. 82, 553–573.

Sposito, G., Prost, R., Gaultier, J.P., 1983. Infrared spectroscopic study of adsorbed water on reduced-charge Na/Li montmorillonites. Clays Clay Miner. 31, 9–16.

Srodon, J., Mccarty, D.K., 2008. Surface area and layer charge of smectite from CEC and EGME/H_2O-retention measurements. Clays Clay Miner. 56, 155–174.

Steudel, A., Heinzmann, R., Indris, S., Emmerich, K., 2015. CEC and 7Li MAS NMR study of interlayer Li^+ in the montmorillonite-beidellite series at room temperature and after heating. Clays Clay Miner. 63, 337–350.

Swenson, J., Bergman, R., Howells, W.S., 2000. Quasielastic neutron scattering of two-dimensional water in a vermiculite clay. J. Chem. Phys. 113, 2873–2879.

Szczerba, M., Kuligiewicz, A., Derkowski, A., Gionis, V., Chryssikos, G.D., Kalinichev, A.G., 2016. Structure and dynamics of water-smectite interfaces: hydrogen bonding and the origin of the sharp O-D-W/O-H-W infrared band from molecular simulations. Clays Clay Miner. 64, 452–471.

Tainter, C.J., Ni, Y., Shi, L., Skinner, J.L., 2013. Hydrogen bonding and OH^- stretch spectroscopy in water: hexamer (cage), liquid surface, liquid, and ice. J. Phys. Chem. Lett. 4, 12–17.

Tang, M.J., Cziczo, D.J., Grassian, V.H., 2016. Interactions of water with mineral dust aerosol: water adsorption, hygroscopicity, cloud condensation, and ice nucleation. Chem. Rev. 116, 4205–4259.

Tarasevi, Y.I., Gribina, I.A., 1972. Infrared spectroscopic study of state of water in Halloysite. Colloid J. Russ. Acad. of Sci. 34, 346–350.

Tarasevich, Y.I., 2007. The surface energy of hydrophilic and hydrophobic adsorbents. Colloid J. 69, 212–220.

Tarasevich, Y.I., Aksenenko, E.V., 2014. Hydrophobicity of talc basal surface. Colloid J. 76, 483–489.

Tester, C.C., Aloni, S., Gilbert, B., Banfield, J.F., 2016. Short- and long-range attractive forces that influence the structure of montmorillonite osmotic hydrates. Langmuir 32, 12039–12046.

Thompson, C.J., Martin, P.F., Chen, J., Benezeth, P., Schaef, H.T., Rosso, K.M., Felmy, A.R., Loring, J.S., 2014. Automated high-pressure titration system with in situ infrared spectroscopic detection. Rev. Sci. Instrum. 85, 11.

Van Der Vegt, N.F.A., Haldrup, K., Roke, S., Zheng, J., Lund, M., Bakker, H.J., 2016. Water-mediated ion pairing: occurrence and relevance. Chem. Rev. 116, 7626–7641.

Vasconcelos, I.F., Bunker, B.A., Cygan, R.T., 2007. Molecular dynamics modeling of ion adsorption to the basal surfaces of kaolinite. J. Phys. Chem. C 111, 6753–6762.

Veerabadran, N.G., Price, R.R., Lvov, Y.M., 2007. Clay nanotubes for encapsulation and sustained release of drugs. Nano 2, 115–120.

Venyaminov, S.Y., Prendergast, F.G., 1997. Water (H2O and D2O) molar absorptivity in the 1000-4000 cm-1 range and quantitative infrared spectroscopy of aqueous solutions. Anal. Biochem. 248, 234–245.

Verwey, E.J.W., Overbeek, J.T.G., 1948. Theory of the Stability of Lyophobic Colloids. Elsevier, Amsterdam.

Wang, J.W., Kalinichev, A.G., Kirkpatrick, R.J., 2009. Asymmetric hydrogen bonding and orientational ordering of water at hydrophobic and hydrophilic surfaces: a comparison of water/vapor, water/talc, and water/mica interfaces. J. Phys. Chem. C 113, 11077–11085.

Weiss, C.A., Kirkpatrick, R.J., Altaner, S.P., 1990. The structural environments of cations adsorbed onto clays: cesium-133 variable temperature MAS NMR spectroscopy of hectorite. Geochim. Cosmochim. Acta 54, 1655–1669.

Weiss, S., Hirsemann, D., Biersack, B., Ziadeh, M., Muller, A.H.E., Breu, J., 2013. Hybrid Janus particles based on polymer-modified kaolinite. Polymer 54, 1388–1396.

Xu, W., Johnston, C.T., Parker, P., Agnew, S.F., 2000. Infrared study of water sorption on Na-, Li-, Ca- and Mg-exchanged (SWy-1 and SAz-1) montmorillonite. Clays Clay Miner. 48, 120–131.

Yan, L.J., Masliyah, J.H., Xu, Z.H., 2013. Interaction of divalent cations with basal planes and edge surfaces of phyllosilicate minerals: muscovite and talc. J. Colloid Interface Sci. 404, 183–191.

Yariv, S., Shoval, S., 1975. Nature of interaction between water-molecules and kaolin-like layers in hydrated halloysite. Clays Clay Miner. 23, 473–474.

Yin, X., Miller, J.D., 2012. Wettability of kaolinite basal planes based on surface force measurements using atomic force microscopy. Miner. Metall. Process. 29, 13–19.

Yin, X.H., Gupta, V., Du, H., Wang, X.M., Miller, J.D., 2012. Surface charge and wetting characteristics of layered silicate minerals. Adv. Colloid Interface Sci. 179, 43–50.

Zarzycki, P., Gilbert, B., 2016. Long-range interactions restrict water transport in pyrophyllite interlayers. Sci. Rep. 6, 5.

Zecchina, A., Arean, C.O., 1996. Diatomic molecular probes for mid-IR studies of zeolites. Chem. Soc. Rev. 25, 187.

Zeitler, T.R., Greathouse, J.A., Cygan, R.T., 2012. Effects of thermodynamic ensembles and mineral surfaces on interfacial water structure. Phys. Chem. Chem. Phys. 14, 1728–1734.

Zich, D., Zacher, T., Darmo, J., Szocs, V., Lorenc, D., Janek, M., 2013. Far-infrared investigation of kaolinite and halloysite intercalates using terahertz time-domain spectroscopy. Vib. Spectrosc. 69, 1–7.

Zsirka, B., Taborosi, A., Szabo, P., Szilagyi, R.K., Horvath, E., Juzsakova, T., Fertig, D., Kristof, J., 2017. Surface characterization of mechanochemically modified exfoliated halloysite nanoscrolls. Langmuir 33, 3534–3547.